Impurity Effects on Plasma Performance in Two Component Tokamaks

R.W. Conn, M. Khelladi, and J. Kesner

October 1975

UWFDM-136

Submitted to *Nuclear Fusion.*

FUSION TECHNOLOGY INSTITUTE

UNIVERSITY OF WISCONSIN

MADISON WISCONSIN

Impurity Effects on Plasma Performance in Two Component Tokamaks

R.W. Conn, M. Khelladi, and J. Kesner

Fusion Technology Institute
University of Wisconsin
1500 Engineering Drive
Madison, WI 53706

http://fti.neep.wisc.edu

October 1975

UWFDM-136

Submitted to *Nuclear Fusion.*

Impurity Effects on Plasma Performance in Two Component Tokamaks

Robert W. Conn

Mourad Khelladi

Jay Kesner

Fusion Technology Program

Nuclear Engineering Department

University of Wiscinsin

Madison, Wisconsin 53711

UWFDM-136

October 1975

Preprint: Submitted to Nuclear Fusion

Abstract

Impurities and the choice of material for the vacuum chamber liner have important effects on the space and time evolution of the plasma in two component tokamaks. A one dimensional plasma transport program based on a set of fluid equations is used to represent the behavior of the plasma parameters. The equations are time dependent and include the effects of conduction and convection, electric and magnetic field diffusion, ohmic heating, radiative losses, stripping, neutral beam injection, neutral particle transport, recycle at the plasma boundary, and liner sputtering. The important results relate to the role of the initial plasma density and the initial impurity content, the type of impurity, the material chosen for the vacuum chamber liner, and the effects of impurity enhanced neutral beam attenuation. Neglecting this last item, the initial liner impurity content is the dominant effect in determining the maximum Q value. With 15 MW of injected power into a 2.5 MA plasma, Q values of 1 are reached when the initial high Z impurity concentration is less than 0.1% and when the initial plasma density is not greater than about $7 \times 10^{13} cm^{-3}$. Liner sputtering and subsequent impurity radiation affects Q and the energy balance only for times greater than about 500 ms. The effect is minimized by use of a low Z liner. Including 1-2% oxygen together with enhanced neutral beam attenuation caused by impurities alters this conclusion and makes achieving and sustaining Q values near 1 difficult. The maximum initial oxygen concentration for which Q reaches 1 is found to be only 0.5%. In addition, an instability is associated with the impurity enhanced attenuation of the beam since edge heating causes the mean energy of charge exchange neutrals striking the liner to increase. In turn, this increases both the sputtering yield and the impurity reflux to the plasma. The injected beam is further attenuated causing the plasma center to cool and the Q to drop sharply. The instability limits the time period over which Q remains near its maximum value and a low Z liner tends to minimize but does not eliminate this problem. Controlling the sputtering and initial oxygen content is therefore critical to sustaining Q values near or above 1 and the properties of molybdenum as a metallic liner prove to be interesting in this regard.

I. Introduction

Impurities and impurity control is one of the most critical areas in tokamak research and may prove to be the prime factor in the determination of burn times in tokamak reactors. In present experiments, typical impurity concentrations are 1-10% low Z contaminants, primarily oxygen, and 0.05 - 0.2% high Z materials, generally iron.[1-4] Contaminants from the limiter, such as molybdenum and tungsten, are generally present in amounts that are somewhat less than 0.1%. The low Z impurities are present from the beginning of the discharge and remain at a constant level throughout the experiment.

In the next generation of experiments and in larger, reactor size systems, sputtering of the liner by fast charge exchange neutrals or by hot plasma ions can be an important source of such impurities. In turn, these impurities effect the power flows in a tokamak and the overall energy balance as well as the penetration characteristice of neutral beams injected to heat or sustain the plasma. The tolerable impurity levels which a D-T tokamak can withstand while continuing to function as an ignition machine or as a high amplification driven plasma device has recently been studied.[5] The tolerable level of low Z impurities such as carbon is the order of 6% whereas for high Z impurities such as iron, the tolerable level is no more than about 0.2% to maintain an ignited plasma and 0.4-0.6% to allow a high energy amplification factor. It was also noted that driven, two-component tokamaks can withstand somewhat higher levels of high Z impurities.[5] However, such analyses[5,6,7] have been based on global descriptions of the plasma behavior and do not account for important space-dependent effects or for the dynamical aspects of the plasma burn.

Recent work on the two-energy-component tokamak, or TCT,[8] has shown that it is possible to reproduce in fusion power the energy injected into the plasma by neutral beams when the plasma $n\tau_E$ values is about $10^{13} cm^{-3}$-s and the electron temperature is 4.5 keV or greater. In such a machine, fast neutral deuteron beams at energies of about 150 keV are injected into a tritium target plasma maintained at $T_e \gtrsim 4.5$ keV by the beams themselves. Such a device can potentially be a more copious source of neutrons than an ignited D-T plasma machine[9] and is therefore an important candidate for use as a materials and engineering test reactor[10] and for use as the plasma source in fission-fusion hybrids or fissile fuel breeding reactors.

In this paper, we investigate the effect of different vacuum chamber liner materials on the plasma performance and neutral beam penetration characteristics of such two component tokamaks. The plasma energy amplification factor, Q, defined as the power produced by fusion (primarily beam-plasma fusions) divided by the neutral beam power injected onto the plasma target, is chosen as a primary measure of plasma performance. The maximum Q that might be achieved and the time over which Q can be maintained near its maximum value are both studied in detail. For definiteness, we consider a tokamak with dimensions and magnetic field strength characteristics of the conceptual TCT-Tokamak Fusion Test Reactor developed recently.[11] However, the qualitative results are generally applicable to two component plasmas.

In the next section of the paper, the space and time dependent fluid equations used to simulate plasma performance are described. The overall model includes the effects of impurity stripping and radiation, neutral beam injection, and recycled neutral particle transport within the plasma. Also discussed are the models used for the transport coefficients which are input to the simulation equations.

The main characteristics of potential liner materials such as Fe and Mo as well as the low Z materials like C and Be are reviewed in the third section. Fe, Mo, and C have been used for the studies in this paper. In the absence of a divertor, physical sputtering due mainly to charge exchanged neutral particles is the source of impurities to the plasma during the flat top period. Recent measurements on sputtering coefficients that have been used in this paper are thus summarized in this section.

Several different aspects of impurities in tokamaks are considered sequentially in the fourth section in an effort to isolate specific effects. Impurities appear experimentally in the plasma during the first stages of the current rise. The initial impurity concentration is varied first to study the impact of these impurities on the time dependent Q. The actual plasma history during the current rise time is not considered. We then study the effect of various liner materials (Fe, Mo, C) on the time variation of Q assuming the initial impurity concentration is 0.1%. The effect of impurities on the attenuation of the deuteron beam is neglected, as is the presence of oxygen. The effects of the initial oxygen concentrate are then included together with the effect of impurities on the radial variation of the beam energy deposition profile. The initial oxygen concentration is varied from 0.3% to 2% and the initial liner impurity concentration is varied from 0.1% to 0.3%. The reason for choosing these ranges of impurity content is discussed. When all such effects are included together, estimates are made of the tolerable initial impurity content which lead to Q values of about 1 and which allow high Q to be maintained for periods of one second or more. Charge exchange spectra which are important for sputtering studies are also presented.

The anticipated effects of alternate assumptions regarding plasma transport, sputtering yields, and impurity diffusion on the general conclusions are discussed in the last section. Two appendices are included to describe the numerical procedure used to solve the fluid equations and to describe the treatment of neutral particle transport.

II. Fluid Model of Tokamak Plasmas

The tokamak discharge is represented by a set of fluid equations for electrons and ions in cylindrical geometry with spatial dependence admitted in the radial direction. These equations are time dependent and include the effects of conduction and convection of energy and particles, electric and magnetic field diffusion, thermal equilibration between electrons and ions, ohmic heating of the electrons, and plasma radiation losses (bremsstrahlung, synchrotron, line). Furthermore, the numerical program based on these equations takes into account energetic neutral beam injection and heating, amplification of neutral beam energy by fusions of energetic deuterons as they slow down in the tritium plasma, recycling of neutrals, sputtering of the liner, and the stripping, radiation and diffusion of impurities.

The equations to be solved include ion and electron power balance equations, the diffusion equation for ion density, Faraday's Law, Ampere's Law and Ohm's Law. They may be written as follows:

$$\frac{\partial T_e}{\partial t} = 4.28 \times 10^{-11} n_i \frac{(T_i - T_e)}{T_e^{3/2}} + \frac{1}{n_e r} \frac{\partial}{\partial r} (r n_e \chi_e \frac{\partial T_e}{\partial r}) - \frac{S T_e}{n_e}$$

$$- \frac{n_i V_i}{n_e} \frac{\partial T_e}{\partial r} + \frac{4.17 \times 10^{15}}{n_e} \{n_D n_T \langle \sigma v \rangle U_{\alpha e} + \underline{E} \cdot \underline{J} + P_{inj} (U_{be} + f(\frac{E_\alpha}{E_b}) U_{\alpha e})$$

$$- P_I - P_B - P_S - P_L - P_R \} \qquad (1)$$

$$\frac{\partial T_i}{\partial t} = -4.28 \times 10^{-11} n_e \frac{(T_i - T_e)}{T_e^{3/2}} + \frac{1}{n_i r} \frac{\partial}{\partial r} (r n_i \chi_i \frac{\partial T_i}{\partial r}) - \frac{S T_i}{n_i}$$

$$- V_i (\frac{\partial T_i}{\partial r}) + \frac{4.17 \times 10^{15}}{n_i} \{n_D n_T \langle \sigma v \rangle_{DT} U_{\alpha i} + P_{cx} + P_{inj} (U_{bi} + f(\frac{E_\alpha}{E_B}) U_{\alpha i})\} \quad (2)$$

$$\frac{\partial n_i}{\partial t} = - \frac{1}{r} \frac{\partial}{\partial r} (r n_i V_i) \quad (3)$$

$$n_i V_i = -D \frac{\partial n_i}{\partial r} \quad (4)$$

$$\frac{\partial B_\theta}{\partial t} = 10^5 \times \frac{\partial E}{\partial r} \quad (5)$$

$$\frac{\partial J}{\partial t} = 7.96 \times 10^4 \frac{1}{r} \frac{\partial}{\partial r} (r \frac{\partial E}{\partial r}) \quad (6)$$

$$E = \eta_{NC} J \quad (7)$$

$$n_e = n_i + 2n_\alpha + \sum_i n_{Z_i} Z_i \, . \quad (8)$$

$T_{e,(i)}$ is the electron (ion) temperature (eV) B_θ is the poloidal magnetic field (gauss), $n_{e,(i)}$ is the electron (ion) density (cm^{-3}), V_i is the ion velocity (cm/ms), J is the toroidal current density (amp/cm^2), E is the toroidal electric field (volt/cm), r is the radius (cm), t is time (ms), $\chi_{e,(i)}$ is the electron (ion) thermal diffusivity (cm^2/ms), η_{NC} is the neoclassical resistivity (ohm-cm), D is the diffusion coefficient (cm^2/ms), $U_{bi,(e)}$ is the fraction of beam energy going to ions (electrons), $U_{\alpha i,(e)}$ is the fraction of alpha energy going to ions (electrons), and f is the fraction of deuterons in the neutral beam which undergo fusion as they slow down in a tritium target plasma.

P_B, P_S, P_L, and P_R represent bremsstrahlung, synchrotron, line and recombination radiation, respectively (watts), P_{cx} is the energy loss due to charge exchange (watts), and S is the source of cold plasma ($cm^{-3}ms^{-1}$) due to a cold plasma source or neutral particle reflux.

The neoclassical resistivity η_{NL} is given by[12]

$$\eta_{NL} = 0.0103 \quad \frac{\ell n\Lambda}{T_e^{3/2} f_T} \left(\frac{.457\ Z_{eff}}{1.077 + Z_{eff}}\right) + .29\ Z_{eff}) \text{ ohm-cm} \tag{9}$$

with $$f_T = 1 - \{1.95 \sqrt{\frac{r}{R}} + .95\ (r/R)\}/(1 + \nu^*) \tag{9a}$$

$$\nu^* = 6.92 \times 10^{-14}\ Z_{eff}\ \frac{R^{3/2} B_T n_e \ell n\Lambda}{\sqrt{r}\ B\ T_e^{\ 2}} \tag{9b}$$

and

$$Z_{eff} = \frac{\sum n_j Z_j^2}{n_e} \quad . \tag{10}$$

R is the toroidal major radius (cm) and $\ell n\Lambda$ is the coulomb logarithm, f_T is the correction to the resistivity due to particle trapping, and ν^* is the ratio of collision frequency to bounce frequency. The differential equations for the plasma behavior are solved using a symmetric Cranck-Nicholson type method in which the differential equations are linearized and transformed into an implicit set of difference equations.[13]

The transport coefficients (D, χ_e, χ_i) are treated implicitly and are assumed to vary in functional form as the plasma changes in collisionality. The high collisionality regime that is used reflects pseudoclassical scaling[14] and, as the plasma heats, the transport is assumed to be caused by turbulence, passing successively into regimes dominated by the presence of the trapped electron mode,[15] trapped ion mode[16] and the collisionless trapped particle interchange mode.[17] Transport coefficients based on estimates of the linear growth rates for these modes has been summarized by Dean et al.[18] In the

trapped electron regime, the relationship between χ_i and χ_e is not known. Rather than optimistically assuming χ_i remains neoclassical in this regime, we have taken $\chi_i = \varepsilon \chi_e$ where ε is the local aspect ratio.

To allow for a general variation of the transport coefficients, the general form

$$D,\ \chi_e,\ \chi_i = C\ T_e^{S1}\ T_i^{S2}\ n_i^{S3}\ B^{S4}\ (\nabla n)^{S5}\ (\nabla T)^{S6}\ (\nabla q)^{S7}(1 - T_e/T_i)^{S8} \qquad (11)$$

is used in which the coefficients C and S1, S2, . . . , for D, χ_e, or χ_i are determined by the dominant mode present. The exact form of the transport coefficients and the method for differencing the resulting nonlinear terms are given in Appendix 1.

A three dimensional neutral particle transport model has been developed to determine both the spectrum of charge exchange neutrals that impinge on the linear and the loss of plasma energy due to charge exchange. A slab geometry is used since the thickness of the region which neutrals penetrate is much smaller than the plasma minor radius. In this model, the ions diffusing from the plasma and the charge exchange neutrals are recycled at the plasma edge as cold H_2. The H_2 molecules are assumed to dissociate in the outer plasma layer and give rise to Franck-Condon neutrals of 5-10 eV which then penetrate isotropically into the plasma. These neutrals are either ionized by electron or ion impact ionization, suffer a charge exchange which isotropically produces a neutral at the local ion temperature, or escape from the plasma. Particles converted to secondary neutrals by charge exchange continue to be treated for up to 10 generations. Details of this calculation are given in Appendix 2.

The charge-exchange neutrals which escape the plasma will cause sputtering of the liner and will thus be a source of impurities. The sputtering coefficient is energy dependent and we have used a fit to experimental data. This is discussed in Section III.

For carbon or oxygen present in the discharge, a corona model is used to determine the local distribution of these elements at various charge states.[19] Furthermore, the diffusion of these heavy ions was followed by solving a neoclassical transport equation.[20] The corona and impurity transport models were developed by Hogan.[21]

High Z impurities like iron or molybdenum were assumed to distribute themselves uniformly in the plasma and to assume a charge state governed by the local plasma temperature. Recently reported findings on the ST tokamak indicate no selective accumulation of high Z impurities in the center of the plasma even when high Z noble gases such as Xe are admitted during the discharge.[1] The impurity concentration appeared to be fairly uniform. In the calculations reported here, the initial impurity concentrations relative to the electron density (n_{imp}/n_e) were taken to be constant but all impurities sputtered from the liner during the plasma burn time are retained in the plasma. The impurities are assumed to radiate according to the formula,[22,23]

$$W = W_B \left(1 + \frac{37.9\, n_z Z^4}{Z_{eff} n_e T_e} + \frac{860\, n_z Z^6}{Z_{eff} n_e T_e^2}\right) . \qquad (12)$$

Here n_z is the density (cm^{-3}) of impurities in charge state Z and W_B is the bremsstrahlung radiation ($watts/cm^3$),

$$W_B = 1.52 \times 10^{-32}\, n_e^2\, T_e^{1/2} \ (w/cm^3) \quad . \qquad (13)$$

Synchrotron radiation is taken as[25]

$$W_s = 1.6 \times 10^{-28} \left(1 - 0.0305 \frac{R}{a}\right)^3 B_T^{5/2} \sqrt{\frac{n_e}{a}}\, T_e^{2.1} \qquad (15)$$

At low temperatures, eqn. (12) becomes inaccurate and in that case, the formula of Hinnov[24] has been used,

$$W = 1.2 \times 10^{-32} n_z n_e \qquad (14)$$

Which is approximately correct for impurities with three or more electrons remaining. In calculations, the smaller value from eqns. (12) and (14) is used.

The program also calculates the spatial distribution of energy and particles as a result of energetic neutral beam injection.[26] A pencil beam approximation that is considerably less expensive to use is also available.[27] The alpha power generated by beam-plasma fusions which take place as the energetic deuteron slows down in a target plasma containing tritium is taken into account. The calculation of the fraction of beam and alpha energy going to the electrons and ions, and of the plasma β, including the pressure of the high energy particles, follows the procedure we have discussed previously.[5]

III. Sputtering and Liner Materials for Tokamaks

The vacuum vessel or liner material in present day tokamaks is austentic stainless steel. This metal is also projected to be the primary structural material for the next set of large tokamak experiments and for the first generation of tokamak reactors. The use of stainless steel results in the presence of Fe, Cr and Ni in the plasma and these medium weight nuclei constitute high Z impurities from the viewpoint of plasma radiation losses. Such high Z atoms will enter the discharge during the burn time primarily by physical sputtering. Further, the oxygen content with stainless steel liners tends to be 1% or more[1-3] and while such a concentration of O will not lead to a strong increase in radiative losses, the resulting increase in Z_{eff} can have an important impact on neutral beam penetration. This is discussed in the next section. It is thus desirable to reduce both the initial oxygen content and the amount of high Z material sputtered during the plasma burn.

Although stainless steel is the structural material of choice, it is possible to consider nonstructural liners of different materials mounted onto the vacuum vessel or coatings on the stainless steel itself. One may thus consider a number of attractive candidate materials and examine their impact. Fig. 1a is a compilation of sputtering yield data from Rosenberg and Wehner[28] as a function of atomic number for 600 eV He^+. One notes that of the medium weight nuclides, Mo and Nb, have about the lowest sputtering yield (due to the electronic structure of these atoms) and that both have yields that are between 5 and 7 times less than the sputtering yield of Fe or Ni. Fig. 1b is a

compilation of sputtering yield data as a function of Z for H^+ at 3.5 to 3.7 keV from Kenknight and Wehner.[29] The same systematics are observed as for He^+ sputtering and the sputtering yield for Zr and Mo are between 3 and 6 times less than that for the primary constituents of stainless steel. This data would suggest that a refractory metal protective liner could be a useful addition for impurity control.

A further point is that Mo, unlike Nb, is an endothermic metal and will not getter hydrogen or oxygen. Yoshikawa et al.[30] have suggested the use of Mo to permit rapid hydrogen recycle, which would in turn maintain the plasma density. When the Mo is maintained at elevated temperatures (~500°C), oxygen may also be removed from the surface and can therefore be pumped between discharges. The use of Mo thus offers the potential to control the initial oxygen content and to provide rapid recycle of the fuel ions. We have chosen Mo as an alternate liner material for study in addition to Fe.

Carbon has a relatively low physical sputtering coefficient as seen on Figs. 1 and 2 and it offers the advantage over Mo or Fe of being a low Z material. The plasma can tolerate at least an order of magnitude more C than Fe without serious degradation in plasma performance.[5] For these reasons, a stand-off graphite liner has recently been discussed by several groups[31,32] although the question of chemical sputtering remains open. A preliminary study[33,34] indicates that the graphite must be operated either near room temperature or above about 1000°C to minimize chemical reactions. We have chosen graphite as a promising example of a low Z liner.

Data for the sputtering yields of stainless steel, gold, molydenum, and carbon as a function of incident energy are presented in Fig. 2. An analytical fit has been developed by Cohen[35] based on his own low energy sputtering yield data normalized to the values of Behrisch at 5 to 8 keV.[36] The formula is

$$S(E) = \frac{4\, S_{max}\, (E-E_c)^{3/2}\, E_{max}^{1/2}}{(E_{max}^2 + 3\, E^2)} \qquad (16)$$

and we have used this functional form to also represent the sputtering yields from Mo and C, although this point remains to be confirmed experimentally. The values used for S_{max}, E_{max}, and E_c are listed in table 1 assuming the sputtering yield of tritium is three times that for hydrogen and 1.5 times that for deuterium. The sputtering yield given by eqn. (17) is integrated over a Maxwellian to account for the thermal spread of the charge exchanged neutrals.

As a final point, the use of a honeycomb surface on the liner offers the possibility of reducing the sputtering yield by a factor of about 3 compared with a smooth surface.[37] Such a surface pattern can be achieved on most metals by, for example, photoetching. The S_{max} value for Mo is chosen to be five times less than stainless steel. If this reduction turns out experimentally to be only a factor of 2.5 to 3, our calculations would then correspond to a Mo liner with a honeycomb surface where the surface geometry lowers the yield another factor of 2.

TABLE 1

Parameters Used in Eqn. (16) for Sputtering Yield of Tritium on Various Liner Materials

Material	S_{max}	E_{max} (eV)	E_c (eV)
Fe	0.024	6000	23
Mo	0.005	6000	55
C	0.015	6000	5

IV. Results and Analysis

The two component tokamak analyzed in this paper has the same basic characteristics as the conceptual design developed for the tokamak fusion test reactor[11] and the major parameters are summarized in Table 2. At the initial stage, the plasma heats solely by ohmic heating. In the scenario studied here, 100 A of 150 keV neutral deuterium are injected beginning 150 ms after the ohmic heating phase. The 15 MW of beam power is equally divided between injection parallel and antiparallel to the plasma current. While this affords a concrete framework for the discussion, the main results are generally applicable.

Three sequences of calculations have been performed to separately analyze the effect of the initial ion density, the initial impurity content, and the impurity enhanced attenuation of the injected neutral beam, on the space and time dependent evolution of the plasma.

1. Initial Ion Density

The initial plasma density effects both the neutral beam penetration properties, the beam slowing down time, and the losses due to conduction and convection. For a fixed impurity percentage, the initial filling pressure also effects radiation losses. Rutherford[11] has found that for $\frac{n_{imp}}{n_e} \simeq 0.001$ and iron as the impurity, the initial central ion density must be less than about $8 \times 10^{13} cm^{-3}$ to avoid excessive radiative losses which would keep the central temperature less than a few keV. We have not studied this particular effect further.

Fig. 3 summarizes the results of a typical calculation in which the initial ion density has the form

$$n_i(r,t=0) = n_i(0)\left(1 - 0.8\left(\frac{r}{a}\right)^2\right)$$

Table 2

Estimated Parameters of the Conceptual TCT-Tokamak Fusion Test Reactor[11]

MAJOR RADIUS	248 cm
PLASMA RADIUS	85 cm
AXIAL TOROIDAL MAGNETIC FIELD	52 kG
PLASMA CURRENT AT q(a) = 3	2.5 MA
PLASMA COMPOSITION AT t = 0	TRITIUM
NEUTRAL BEAMS	DEUTERIUM
NEUTRAL BEAM ENERGY	150 keV
NEUTRAL BEAM INJECTED POWER	15 MW

with $n_i(0) = 7 \times 10^{13} cm^{-3}$. For this case, a carbon liner is assumed and the neutral beam deposition profile is calculated assuming $Z_{eff} = 1$. The central ion temperature rises quickly and exceeds 10 keV after about 500 ms. Although the electron temperature is greater than the ion temperature at early times, it does not reach as high a value because the beams deposit a larger fraction of their energy in the ions as T_e increases. The thermonuclear amplification factor, Q, exceeds 1 after about 375 ms but begins to decrease slowly from its maximum value after about 600 ms. This decrease is related to the ion density increase resulting from the injection of deuterium. While the tritium density remains constant, the ion density increase causes the slowing down time and the probability of beam plasma fusion to decrease. The electron and ion temperatures peak and also begin to drop because the same amount of injected power (15 MW) is now distributed over more particles. This also contributes to the decrease in Q. Maxwellian fusions become relevant as the deuterium content increases but they are not sufficient to offset these other effects. The chronology of events outlined here is found in all the calculations, including those where inpurities play a more detrimental role.

Fig. 4 shows results for the same discharge scenario but with $n_i(0)$ initially at $10^{14} cm^{-3}$. In this case, the average electron temperature does not exceed 2.5 keV and the maximum Q is about 0.85, or 20% less than in the previous case. If the initial 0.1% impurity content had been made up of Fe rather than C, the average temperatures would not have exceeded 1 keV, as found by Rutherford.[11] As a consequence of these results, the initial ion density is set equal to 7×10^{13} ions/cm^3 for the following studies.

2. Liner Sputtering Effects on TCT Performance

The effects of different liner materials is summarized in Fig. 5, again without including the effects of impurities on the beam deposition profile. The initial impurity content is 0.1% of the average electron density and the impurities are distributed with the same initial profile as the ions and electrons. All cases reach a Q of about 1 at 500 ms but the Fe liner case shows Q beginning to drop more rapidly after about 600 ms. This is caused by the more rapid increase in iron content as compared to molybdenum and is related directly to the difference in sputtering yields. (See Fig. 2). Interestingly, the average electron temperature is approximately the same with C, Fe, or Mo liners (~3.5 keV). The reason is that radiation losses are not dominant and the sputtering yields do not dramatically increase the impurity level during the one second period. In the worst case considered here (Fe) the maximum impurity content increases from $7 \times 10^{10} cm^{-3}$ to only $1.2 \times 10^{11} cm^{-3}$ in 800 ms. The increase in the case of a Mo liner is much less.

One can conclude, neglecting the effects of impurities on beam penetration, that physical sputtering significantly effects a TCT plasma of 2.5 MA rating only for times greater than one second. The impurity influx is slow because, at the beam energies used, the central core of the plasma is preferentially heated and plasma near the edge remains relatively cold and in the pseudo-classical regime. This keeps the recycle of neutrals relatively low. Note again that sputtering is due to charge exchange neutrals and not to plasma particles diffusing across the plasma boundary.

The effect of impurities on the neutral beam deposition profile can alter this conclusion. The ion impact ionization cross section is the most important for trapping deuterons at 150 keV. When impurities are present in a plasma,

this cross section is proportional to Z_{eff}.[38]

The neutral beam deposition profile at two different times is shown in Fig. (6) for the case of an iron liner with the initial impurity concentration equal to 0.1%. At 200 and 350ms, the profile remains peaked at the center. At the later time, 750 ms, the profile is flatter and peaks at about two thirds of the plasma radius. The central peak is dramatically reduced.

The central peaking at early times occurs because the plasma is not yet hot enough to significantly strip high Z impurities. As a result, the Z_{eff} remains close to 1, as seen in Fig. (6a). The stripping level of a high Z impurity has been taken as $\bar{Z} = \left(\frac{T_e}{13.6} \right)^{1/2}$ for T_e in eV. The maximum Z_{eff} of about 2 is obtained later in the discharge and causes the flatter beam deposition profile shown at 750ms.

The ion temperature profile at 700ms with and without the effect of impurities on beam penetration is shown in Fig.(7). The temperatures within 10-15cm of the plasma edge, where charge exchange is most important, is substantially higher by 0.5 - 1 keV when the effect of impurities on beam penetration is included.

The time history of the main plasma parameters for this case is shown in Fig. (8). The Q value reaches about 1 at 500ms but quickly begins to decrease and is less than 0.8 at 700ms. A comparison with the results in Fig. (5), shows that for times less than 500ms, the major plasma parameters are about the same. The reason is the iron is not yet highly stripped. However, in the later stages, the beam deposition profile has become flatter and the outer regions of the plasma are preferentially heated. If the trapped electron mode is present, preferential edge heating leads to higher particle diffusion rates,

and a larger charge exchange neutral flux to the liner. The enhanced sputtering increases Z_{eff} and causes the beam to attenuate even closer to the edge. This leads in turn to an even larger particle flux from the plasma, a further increase in sputtering, and so on.

Thus, there is an instability related to impurity enhanced attenuation of the injected neutral beam which leads to rapid cooling of the discharge and terminates with the cooling of the plasma edge by excessive impurity influx and radiation. This instability limits the time period for which Q remains near its maximum value and for the case at hand, Q exceeded 0.9 for only about 200ms.

When the initial iron content is higher, the overall effect is slightly different. The maximum values of Q and average electron temperatures are given in Table 3 for three cases where the initial impurity content is 0.1%, 0.2% and 0.3% iron. The maximum Q drops by 15-20% each time the initial Fe content increased by 0.1%. Of course, the maximum $\bar{T}_e$ also decreases. On the other hand, the instability leading to enhanced sputtering is somewhat less severe in the latter two cases (0.2 and 0.3% Fe) because the electron temperatures are lower and the particle leakage rate is less. This can be seen in Fig. (9) where the iron impurity content is plotted as a function of time. For times greater than about 600ms, the iron concentration actually becomes largest for the case which began with the smallest initial impurity content.

It therefore appears that the maximum initial iron content which allows Q to reach about 1 is 0.1%. This result would be the same for a molybdenum

Table 3

Variation of Maximum Q and Maximum $\bar{T}_e$ with Initial Fe Impurity Content

INITIAL Fe Content	$\bar{T}_e^{max}$ (keV)	Q^{max}
0.1%	3.3	1.0
0.2%	3.1	0.85
0.3%	2.7	0.70

liner because radiation losses are insensitive to the type of high Z impurity at the electron temperature levels reached.[24] However, since the sputtering yield of molybdenum is three to five times less than that for stainless steel, the instability provoking enhanced sputtering will not be as severe and Q can remain near Q^{max} for longer times. We investigate this later in the paper.

3. Role of Liner Sputtering and Oxygen on TCT Performance

In present tokamak experiments with stainless steel liners, the oxygen concentration is typically 1-2% and can be as much as 10%.[1-3] Such concentrations of low Z impurities will have an important effect on neutral beam penetration and on the consequences which follow from enhanced sputtering. We consider first the case where the initial oxygen content is 2%, the liner is Fe, but there is no initial iron impurity content. The initial Z_{eff} is about 2 and is the same as the Z_{eff} produced by 0.1% Fe when the impurity is fully stripped.

The neutral beam deposition profile and the value of Z_{eff} are shown as a function of radius in Fig. (10) at 350ms and 700ms into the discharge. In contrast with the earlier case (see Fig. 6), the beam deposition profile is relatively flat at both 350ms and 700ms. The reason is the oxygen is readily stripped (T_e ~600eV is required) and the full Z_{eff} is developed quickly. The consequence is the early time heating of the outer plasma regions which produces greater conduction and convection losses. Thus, as shown in Fig. (11), a lower value of $\bar{T}_e^{max}$ is found (~3.1 keV) and the maximum value of Q is 0.77. These values are lower than in the case where oxygen is neglected and the initial iron content is 0.1% (see Fig. (8) or table 3). The lower values cannot be explained simply by the lower average electron temperature achieved (3.1 keV versus 3.3 keV). In fact, the plasma heats more slowly because of the enhanced

beam attenuation and the maximum Q is reached at about 1000ms rather than 500ms. At such late times, the ion density has increased, the slowing down time for the beam has decreased, and the resulting Q value is lower. This effect was discussed earlier in section IV-1.

The results for a low Z carbon liner and 2% initial oxygen content are also shown on Fig. (11). (Since oxygen and carbon radiate similarly once stripped, this is essentially equivalent to beginning with 2% C and a carbon liner.) The Q value is now a slowly increasing function of time and reaches 0.85 at one second. Radiative losses are not a significant factor in the overall plasma power balance.

It is of interest to determine the maximum initial oxygen content which leads to Q ~ 1 with a metallic liner. Molybdenum is used for reasons which will be discussed shortly and it is found that 0.5% initial oxygen content allows Q to reach 1 (see Fig. (11)). At this oxygen concentration, the neutral beam at 150 keV penetrates adequately, heats the center and yields a maximum space averaged electron temperature of 3.6 keV.

4. β_θ,Γ, and the Neutral Flux to the Liner

Two parameters of special interest in beam driven tokamaks are the poloidal beta, β_θ, and Γ, the ratio of the pressure excited by the high energy beam injected particles to the background plasma pressure. The expression for Γ is

$$\Gamma = \frac{\frac{2}{3} n_F W_B}{(n_i T_i + n_e T_e)}$$

where n_F is the number of suprathermal ions given by $I_B \tau_{SD}$. I_B is the beam injection current, τ_{SD} is the slowing down time, and W_B is the injection energy. For the simpliest case where the beam injected power balances all losses, the expression for Γ is

$$\Gamma = \frac{\tau_s}{\tau_E}$$

where τ_E is the overall energy containment time. An average gamma, $\bar{\Gamma}$, defined in terms of the average energy of the superathermal ions, $\overline{W_B}$, is sometimes used. Since $\overline{W_B} \simeq 1/2\ W_B$, it follows that $\bar{\Gamma} \simeq 1/2\ \Gamma$.

β_θ and $\bar{\Gamma}$ are plotted as a function of time in Fig. (12) for the case of 0.5% initial oxygen content and a Mo liner. β_θ is slowly increasing over the period of the calculation and reaches a relatively low value of about 0.8. $\bar{\Gamma}$ increases sharply just after the beams are turned on because the background plasma pressure is lowest there. However, the maximum value is 0.45 and this too is reasonable from the viewpoint of beam induced instabilities.[39]

Fig. (13) shows the variation with time of the different contributions to the overall plasma energy balance. Radiation and charge exchange losses, although increasing sharply with time, are on order of magnitude less than the conduction and convection losses. These last two terms also increase sharply with time because of the transition from the pseudoclassical scaling at early times to the trapped particle regimes as the plasma heats up.

The energy spectrum of neutral particles incident on the liner is an important quantity, particularly to those concerned with plasma wall interactions in tokamaks. Fig. (14) shows this spectrum at two different times, 300ms and 970ms. One can see that at the later time, particles with energies from 100eV to 4000eV can contribute to liner sputtering and that the maximum wall flux of $\sim 10^{15}$ particles/cm^2-s occurs at low energy, as expected. In addition, the flux of particles with energies greater than 1 keV is less than about 4×10^{14} particles/cm^2-s. If the transport scaling had remained pseudoclassical, the fluxes at long times would be lower with maximum values similar to the results in Fig. (14) at 300ms.

5. A Special Case

A molybdenum liner may be advantageous because its sputtering yield is lower than that for stainless steel, it is compatible with a vacuum environment, it has excellent high temperature properties, and it is endothermic with respect to its interaction with hydrogen and oxygen. As discussed by Yoshikawa et al.[30] and reviewed in Section III, the use of Mo at about 500°C should permit rapid recycle of hydrogen while allowing control of the initial oxygen content.

To examine the impact of a liner with such properties on the performance of a two component tokamak, we have studied a space-time history for the TFTR plasma at 2.5 MA in which the initial oxygen content is 0.3% and the initial molybdenum content is 0.07%. 15 MW of 150 keV deuteron beams are turned on at 150 ms after the ohmic heating phase, as in all previous cases. We have carried the calculation out to an equivalent discharge time of two seconds. The results are given in Fig. 15.

The maximum Q is 1.13 at 950 ms and the Q value is maintained above 0.9 for 600 ms. The average electron and ion temperatures reach maximum values of 4.0 keV and 5.0 keV, respectively. The slow decrease in both Q and $\bar{T}_e$ is caused primarily by the buildup of deuterium in the plasma rather than by liner sputtering. The time interval of 600 ms when Q exceeds 0.9 is quite large compared with all previous cases and points to the importance of controlling the initial impurity content when a metallic liner is employed.

V. Conclusions

Impurities and the choice of liner material can have important effects on the space and time evolution of a plasma in two component tokamaks. Three sequences of calculations have been performed to separately analyze the role of the initial plasma density, the initial impurity content, the effect of impurity enhanced attenuation of the injected neutral beam, and the choice of liner material. Stainless steel (iron), molybdenum, and graphite have been studied as potential liners. The source of impurities during the discharge is physical sputtering by charge exchange neutrals and the specific TCT device used as an example has parameters typical of next generation tokamak experiments (I_p = 2.5 MA). The results, however, are generally applicable to two component devices.

For the first problem, it is found that the initial ion density has a significant effect on the Q value when the amount of injection power is held fixed. The maximum central ion density for which Q reaches 1 is about $7 \times 10^{13} cm^{-3}$. The reason is that the injection power essentially balances all losses. As such, the overall energy balance in the presence of rapid transport caused by trapped particle scaling leads to lower average electron temperatures when the density of particles increases. In a similar vain, it is also found that Q begins to drop at relatively long times (t > 500ms) because the neutral injection produces a slow buildup of deuterium in the plasma and an increase in the total ion density.

Should the scaling be pseudoclassical in large tokamaks, this result would change. In particular, the energy confinement would be much better so that, as the initial density increases, the plasma temperature would increase

more slowly but would nevertheless reach the values required to achieve Q about 1.

Impurities have an important effect on the attenuation of the injected neutral beam. As Z_{eff} increases, the beam deposition profile shifts from being peaked on axis to being either relatively flat or actually peaked near the plasma edge. When this effect is neglected, one finds a rapid increase in Q and maximum Q values near or above 1, regardless of the liner material (Fe, Mo, or C). The reason is the plasma center heats significantly while the edge remains relatively cool. A cool edge minimizes physical sputtering and it is found that the impurity influx over a one second period would not significantly effect a TCT.

However, properly accounting for the effect of impurities on the neutral beam energy deposition profile significantly alters this conclusion. Beginning with 0.1% liner impurity but no oxygen in the plasma, the Q value is found to increase sharply once the neutral beams are turned on and to reach a maximum value near 1 in about 350 ms. This is because at early times, when T_e is relatively low, high Z impurities are not fully stripped and Z_{eff} is close to 1. As T_e increases, Z_{eff} increases causing more of the neutral beam to be attenuated in the outer regions of the plasma. Such enhanced attenuation results in higher temperatures in the edge region where the neutral density is highest. In turn, this leads to higher energy charge exchange neutral particles incident on the liner, increasing both the sputtering yield and the impurity reflux to the plasma. Such a sequence of events is unstable since it leads to a further increase in Z_{eff} near the edge and a more rapid

attenuation of the neutral beam. The instability is terminated by rapid cooling of the central region, a sharp decrease in Q, and finally the cooling of the edge due to an excessive impurity content. One practical consequence of this instability is the limit it places on the time for which Q remains near its maximum value. For the specific case we have studied, Q exceeded 0.9 for only 200ms and dropped rapidly after that. We also find that the maximum initial high Z content for which Q reaches 1 is about 0.1%.

Compared to a metal liner, a low Z liner does not produce quite as severe a problem because the Z_{eff} associated with a given impurity concentration is lower. As such, the beam penetrates more effectively and the problem of excessive edge heating is minimized.

Oxygen is an important contaminant in present day tokamaks. When we include an initial oxygen content of 2% together with a stainless steel liner, the plasma is found to heat more slowly because the oxygen strips quickly and acts to attenuate the injected beam. When the liner is a low Z material, the plasma heats slowly but does reach a somewhat higher Q value because radiative losses and beam attenuation are not as severe. In general, the largest initial oxygen content for which Q reaches 1 with a metallic liner is found to be only about 0.5%. This may in fact be difficult to achieve experimentally.

In this connection, a molybdenum liner may have special advantages because its sputtering yield is lower than that for stainless steel, it is compatible with a vacuum environment, it has excellent high temperature properties, and it is endothermic with respect to interactions with oxygen and hydrogen.[30] This last property should permit rapid recycle of the hydrogenic fuel while allowing control of the initial oxygen content.

The space-time simulation of such a case (0.3% O and 0.07% Mo at time zero) shows that the maximum Q exceeds 1 and that Q is greater than 0.9 for 600 ms. This is a long plateau time compared with all previous cases and points to the importance of controlling the initial impurity content when the vacuum chamber or its liner is metallic.

Acknowledgement

Research supported by the U. S. Energy Research and Development Administration (Contract AT(11-1)-2272) and the Wisconsin Electric Utilities Research Foundation. The authors also wish to thank Dr. John Hogan of Oak Ridge National Laboratory, Dr. Paul Rutherford of the Princeton Plasma Physics Laboratory , and Dr. John Sheffield of the Culham Laboratory for several relevant discussions.

Appendix 1

Transport Coefficients

The transport coefficients are chosen under the assumption that as the plasma becomes more collisionless it will pass spontaneously from neoclassical ion scaling and pseudoclassical electron scaling into regimes dominated by the trapped electron mode, trapped ion mode, and finally the trapped particle interchange mode. The neoclassical ion and pseudoclassical electron transport coefficients are multiplied by constants so as to match the transport coefficients observed at Oak Ridge.[21] The diffusion coefficients (D) and the thermal diffusivities (χ_e, χ_i) take the following forms:[18]

Neoclassical Ions, Pseudoclassical Electrons ;

$$\chi_e = 7.8 \times 10^{-5}\ n\ Z_{eff}\ \ell n\Lambda / B^2 T_e^{1/2} \tag{A1}$$

$$\chi_i = 2.2 \times 10^{-4} \left(\frac{A_m r}{R T_i}\right)^{1/2} \frac{n \ell n \Lambda}{B^2} \tag{A2}$$

$$D = 2.2 \times 10^{-5}\ n\ Z_{eff}\ \ell n\Lambda / B^2 T_e^{1/2} \tag{A3}$$

Dissipative Trapped Electron Mode 1 ;

$$\chi_e = 6 \times 10^{20} \left(\frac{r}{R}\right)^{3/2} \frac{\nabla n\ \nabla T\ T_e^{5/2}}{n^2\ B_T^2\ Z_{eff}} \tag{A4}$$

$$\chi_i = D = \left(\frac{r}{R}\right) \times \chi_e \tag{A5}$$

Dissipative Trapped Electron Mode-2 (lower frequency regime of trapped electron mode);

$$\chi_e = .062 \left(\frac{r}{R}\right)^{1/2} A_m (q(r)/\nabla q) \frac{n_e \nabla T\ Z_{eff}}{B_T^2\ T_e^{3/2}} \tag{A6}$$

$$\chi_i = D = \left(\frac{r}{R}\right) \times \chi_e \qquad (A7)$$

Trapped Ion Mode ;

$$D = \chi_i = \chi_e = 2 \times 10^{20} \frac{(r/R)^{5/2} T_e (r)^{7/2} \left(\frac{\nabla n}{n}\right)^2}{n_e (1 + T_e/T_i)^2 Z_{eff} B_T^2} \qquad (A8)$$

Collisionless Trapped Particle Interchange Mode;

$$D = \chi_e = \chi_i = 10^8 \frac{T_e(r)}{\sqrt{2}\, B_T} \frac{r^{5/4}}{R^{3/4}} (\nabla n/n)^{1/2} \qquad (A9)$$

Here A_m is the ion mass and B_T is the toroidal magnetic field (gauss).

Clearly, the transport coefficients can be expressed in the form given by eqn.(11). By expressing q and Δq interms of B and ΔB, and the gradients in terms of the appropriate differences, the transport coefficients represent nonlinear functions of the seven dependent variables (T_e, T_i, E, B, J, N_i, V_i). Following the method of Widner and Dory,[13] the equations are linearized and time derivatives are evaluated half a step forward to create an implicit tridiagonal set of linear equations which can then be solved at each time step by a matrix inversion. For example, consider an equation of the form

$$\frac{\partial T_e}{\partial t} = F(T_e, T_i, J, B, E, n_i, V_i) \qquad (A10)$$

where F is a non-linear function of the seven variables. This is written as

$$\frac{\partial T_e}{\partial t} = 1/2(F^N + F^{N+1}) \qquad (A11)$$

where F^N is the former value of F and F^{N+1} is its new value. The last step is to evaluate F^{N+1} as

$$F^{N+1} = F^N + \partial t\left(\left(\frac{\partial F}{\partial T_e}\right)^N \frac{\partial T_e}{\partial t} + \left(\frac{\partial F}{\partial T_i}\right)^N \frac{\partial T_i}{\partial t} + \left(\frac{\partial F}{\partial J}\right)^N \frac{\partial J}{\partial t} + \ldots\right) \qquad (A12)$$

where the derivatives of F with respect to the other dependent variables are taken at the previous time and the time derivatives are evaluated implicitly.

Appendix 2

Neutral Model

A three dimensional model has been developed to aid in these studies. Since the neutrals can penetrate only a small distance into the plasma compared with the plasma minor radius, a slab geometry serves as a good approximation. The azimuthal angle is included and the transport is azimuthally symmetric.

The source of cold gas into the plasma is controllable (by regulating the pressure of the gas surrounding the plasma) but in these calculations, the ions which diffuse from the plasma and the escaping charge exchange neutrals are recycled as cold (.03 eV) H_2 molecules.

The H_2 molecules enter the plasma and undergo Franck-Condon dissociation in the outer plasma layer, giving rise to an isotropic source of neutrals in the 1 to 5 eV range,

$$H_2 + \bar{e} \rightarrow H^+ + H_o + 2\bar{e} \ . \qquad \text{(A13)}$$

where the barred quantities represent energetic particles. This reaction requires 30 eV and thus serves to cool the electrons at the plasma edge. The ions and electrons produced in this process are taken account of in the density balance.

The neutrals that are produced in this way can enter the plasma and may undergo either electron or ion impact ionization or charge exchange:

$$H^o + \bar{e} \rightarrow H^+ + \bar{e} + e \qquad \text{(A14)}$$

$$H^o + \bar{H}^+ \rightarrow H^+ + \bar{H}^o + e \qquad \text{(A15)}$$

$$H^o + \bar{H} \rightarrow H^+ + \bar{H}^o \qquad \text{(A16)}$$

The impact ionizations are accounted for in both the density and energy balance (an energy of 13.6 eV is required for ionization). Charge exchange effects only the energy balance, and creates a secondary hot neutral. These second generation neutrals are considered to be monoenergetic at the local temperature and isotropic. They also can undergo either impact ionization, charge exchange, or escape from the plasma. Generally, 10 generations of neutrals are followed.

The cross sections used in these calculationa are taken from Riviere and $\langle\sigma v\rangle$ is calculated by averaging the monoenergetic neutrals over a Maxwellian ion distribution at the local plasma temperature.

In formulating the problem mathematically, we assume that the outer region of the plasma is divided into a number of layers of equal thickness (h), the center point of which corresponds to the grid points of the main spacial mesh. The neutrals produced by charge exchange are assumed to originate from the center of each layer considered. This given a source S(K) for each generation of neutrals coming from the K^{th} layer. Within layer I, the attenuation of the source from layer K which is in the solid angle $d\Omega$ is then given by

$$\delta A_{KI} = S(K)\frac{d\Omega}{4\pi}\{\exp[-\frac{h}{\cos\theta}[-\frac{1}{2\lambda_K} + \sum_{j=K+1}^{I-1}\frac{1}{\lambda_j}]] - \exp[-\frac{h}{\cos\theta}[\frac{1}{2\lambda_K} + \sum_{j=K+1}^{I}\frac{1}{\lambda j}]]\} \quad A17$$

where h is the thickness of each layer, λ_j is the attenuation length defined by $\lambda_j = \frac{V(K)}{n_j\langle\sigma v\rangle_{tot}}$, V(K) being the thermal velocity of the neutrals created in the K layer, n_j the density of the j^{th} layer, and $\langle\sigma v\rangle_{tot}$ the total cross section for ionization and charge exchange in the j^{th} layer. The total attenuation of all neutrals that takes place in layer I is then given by A_I:

$$A_I = \sum_{K \neq I} \int_o^{\pi/2} \delta \, A_{KI} \sin\theta \, d\theta \qquad \text{(A18)}$$

The integration is carried out by means of Gaussian quadrature. The fraction of neutrals which are ionized is $\frac{\langle\sigma v\rangle_{ion}}{\langle\sigma v\rangle_{tot}} A_I$ and the fraction which are charge exchanged is $\frac{\langle\sigma v\rangle_{cx}}{\langle\sigma v\rangle_{tot}} A_I$. This last quantity serves as the source for the next generation of neutrals.

REFERENCES

1. S. Von Goeler, W. Stodiek, H. Eubank, H. Fishman, S. Grehenshchikov, E. Hinnov, Nuclear Fusion 15, (1975) 301.

2. F. DeMarco, "Impurity Concentration in ATC," Princeton Plasma Physics Lab. Report, MATT-1012 (Nov., 1973).

3. P. E. Stott, C. C. Daughney, R. A. Ellis, Jr., Nuclear Fusion 15, (1975)431.

4. H. K. Forsen et al., "Configuration Optimization and Impurity Control in Tokamaks," Energy Research and Development Administration Report, ERDA-6 (June, 1974).

5. R. W. Conn, J. Kesner, Nuclear Fusion (in press.)

6. D. Meade, Nuclear Fusion 14 (1974) 289.

7. D. L. Jassby, "Optimization of Fusion Power Density in the Two Energy Component Tokamak Reactor," Princeton Plasma Phys. Lab. Report, MATT-1072(1974).

8. J. M. Dawson, H. P. Furth, F. Tenney, Phys. Rev. Letts. 26 (1971) 1156.

9. D. L. Jassby, Nuclear Fusion 15 (1975) 453.

10. R. W. Conn, D. L. Jassby, "A Tokamak Engineering Test Reactor," Joint University of Wisconsin-Princeton Plasma Physics Lab. Report, UWFDM-119, MATT-1155 (Aug, 1975).

11. Two Component Torus, Joint Conceptual Design Study, (Princeton Plasma Physics Laboratory and Westinghouse Electric Corp., June 1975) Vols. I, II, and III.

12. R. Hazeltine, F. Hinton, M. Rosenbluth, Phys. Fluids, 16 (1973) 1645.

13. M. M. Widner, R. A. Dory, Bull. Am. Phys. Soc. 11 (1970) 1418. See also, Oak Ridge Nat'l Lab. Report ORNL-TM-3498 (1971).

14. L. Artsimovich, J.E.T.P. Letts. 13 (1971) 70.

15. B. B. Kadomtsev, O. P. Pogutse, Nuclear Fusion 11 (1971) 67.

16. B. B. Kadomtsev, O. R. Pogutse, Sov. Phys. Dokl. 14 (1969) 470.

17. J. D. Callen, B. Coppi, R. Dagazian, R. Gajewski, D. J. Sigmar, in Plasma Physics and Controlled Nuclear Fusion Research (Proc. Madison Conf., June, 1971) (IAEA,Vienna, 1972) Vol. II, p. 451.

18. S. O. Dean et al. "Status and Objectives of Tokamak Systems for Fusion Research," U.S. Atomic Energy Commission, WASH-1295 (1974).

19. J. T. Hogan, Oak Ridge National Laboratory, Private Communication.

20. J. W. Conner, Plasma Physics 15 (1973) 765.

21. J. T. Hogan, Oak Ridge National Laboratory, Private Communication.

22. A. P. Vasil'ev, G. G. Dolgov - Savel'ov, V. I. Kogan, Nuclear Fusion Suppl., pg 2 (1962) 655.

23. G. R. Hopkins, "Impurity Radiation Loss Mechanism from Fuson Reactor Plasmas, Gulf General Atomic Co. Report, G. A. 12374 (Oct. 1972).

24. E. Hinnov, Plasma Physics 14 (1972) 755, See also Princeton Plasma Physics Lab. Report, MATT 777 (1970).

25. T. F. Yang et al., "The Calculation and Parametric Study of Synchrotron Radiation Loss from Tokamak Reactors," Nucl. Eng. Dept. Report UWFDM-49 (The University of Wisconsin, 1973).

26. J. A. Rome, J. D. Callen, J. F. Clarke, Nuclear Fusion 14 (1974) 141.

27. D. G. McAlees, R. W. Conn, Nuclear Fusion 14 (1974) 419.

28. D. Rosenberg, G. K. Wehner, J. Appl. Phys. 33 (1962) 1842.

29. C. E. Kenknight, G. K. Wehner, J. Appl. Phys. 35 (1964) 322.

30. M. Yoshikawa et al., "The JT-60 Program," presented at IAEA Meeting of Specialists on Large Tokamak Experiments (July, 1975).

31. G. L. Kulcinski, R. W. Conn, G. Lang, Nuclear Fusion 15 (1975) 327.

32. GAC Fusion Engineering Staff, "Experimental Power Reactor Conceptual Design Study," General Atomic Report GA-A13534 (July 1975).

33. G. R. Hopkins, D. Kearney, L. Rovner, Trans. Am. Nucl. Soc. 21 (1975) 54.

34. I. P. Busharov, E. A. Gorbatov, V. M. Gusev, M. I. Guseva, Yu. Y. Martynenko, "Chemical Atomization of Graphite by H^+ Ions," Kurchatov Institute of Atomic Energy Report (Moscow, 1975). ERDA Translation, ERDA-TR-50.

35. S. Cohen, cited in D. Meade et al. "The Effects of Impurities and Magnetic Divertors on High Temperature Tokamaks," in Plasma Physics and Controlled Nuclear Fusion Research (Tokyo Conf., Nov. 1974) paper CN-33/A15-4.

36. R. Behrisch, private communication.

37. S. N. Cramer, E. M. Oblow, Nuclear Fusion 15 (1975) 339.

38. E. W. McDaniel, Collision Phynomena in Ionized Gases (John Wiley and Sons, New York, 1964). Also, Dr. John Hogan & Dr. John Sheffield, private communication.

39. H. L. Berk et al., "Two Energy Component Toroidal Fusion Devices." in Plasma Physics and Controlled Nuclear Fusion REsearch (Tokyo Conf., Nov, 1974) paper CN-33/G2-3.

40. A. C. Riviere, Nuclear Fusion 13 (1971) 367.

Figure Captions

Figure 1 - a. Sputtering yield in atoms per ion for 600 eV He^+ as a function of atomic number.
b. The measured sputtering yield for H^+ in the 3.5-3.7 keV range as a function of atomic number.

Figure 2 - Sputtering yield in atoms per ion for D^+ incident on gold, 304 stainless steel, carbon, and molybdenum. The solid lines represent a fit based on eqn. (16).

Figure 3 - Time history of the plasma parameters in a TCT with I_p = 2.5 MA with 15 MW of injected power at 150 keV. The central and average temperatures, the average ion density, and the energy amplification factor, Q, are shown as a function of time. The initial ion density is $7 \times 10^{13} cm^{-3}$.

Figure 4 - Similar to Figure 3 except the initial ion density is $1 \times 10^{14} cm^{-3}$. Note the drop in Q, $T_e(o)$, and $T_i(o)$ compared to the case where the initial ion density is $7 \times 10^{13} cm^{-3}$.

Figure 5 - The effect of various liner materials on the major plasma parameters in a TCT. The effect of impurities on the attenuation of the neutral beam is neglected. The sharp increase in $\bar{n}_{imp}$ for Fe is due to its higher sputtering yield compared to Mo.

Figure 6 - Z_{eff} and the neutral beam attenuation profile in the plasma at various times. The beams are turned on at 150 ms.

Figure 7 - The election and ion temperature radial profiles at two different times. In the upper figure, the effects of impurities on beam attenuation has been neglected.

Figure 8 - Time history of the plasma parameters in a 2.5 MA TCT with an iron liner. The sharp drop in Q after 500 ms is due to the influx of impurities which prevents the beam from penetrating adequately into the plasma.

Figure 9 - The average impurity concentration as a function of time for several initial impurity concentrations.

Figure 10 - Z_{eff} and the neutral beam deposition profile in a 2.5 MA TCT plasma with a 2% initial oxygen content and 0.1% Fe content.

Figure 11 - Time history of the plasma parameters in a TCT as a function of the initial oxygen content and the type of liner. Note that with the low Z liner, Q is slowly but continuously increasing over the 1 second period.

Figure 12 - Different contributions to the power losses from the plasma as a function of time for the case of 0.5% oxygen and a Mo liner. The losses are dominated by conduction and convection when trapped particle instabilities are assumed to govern the plasma transport.

Figure 13 - The poloidal beta and $\bar{\Gamma}$ as a function of time in the TCT. Γ is approximately twice $\bar{\Gamma}$.

Figure 14 - The flux of neutral particles incident on the liner of a 2.5 MA TCT as a function of neutral particle energy at two different times during the model discharge.

Figure 15 - Q, $\bar{T}_i$, and $\bar{T}_e$ as a function of time in a TCT where the initial oxygen content is low (0.3%) and the liner is molybdenum which has a low sputtering yield.

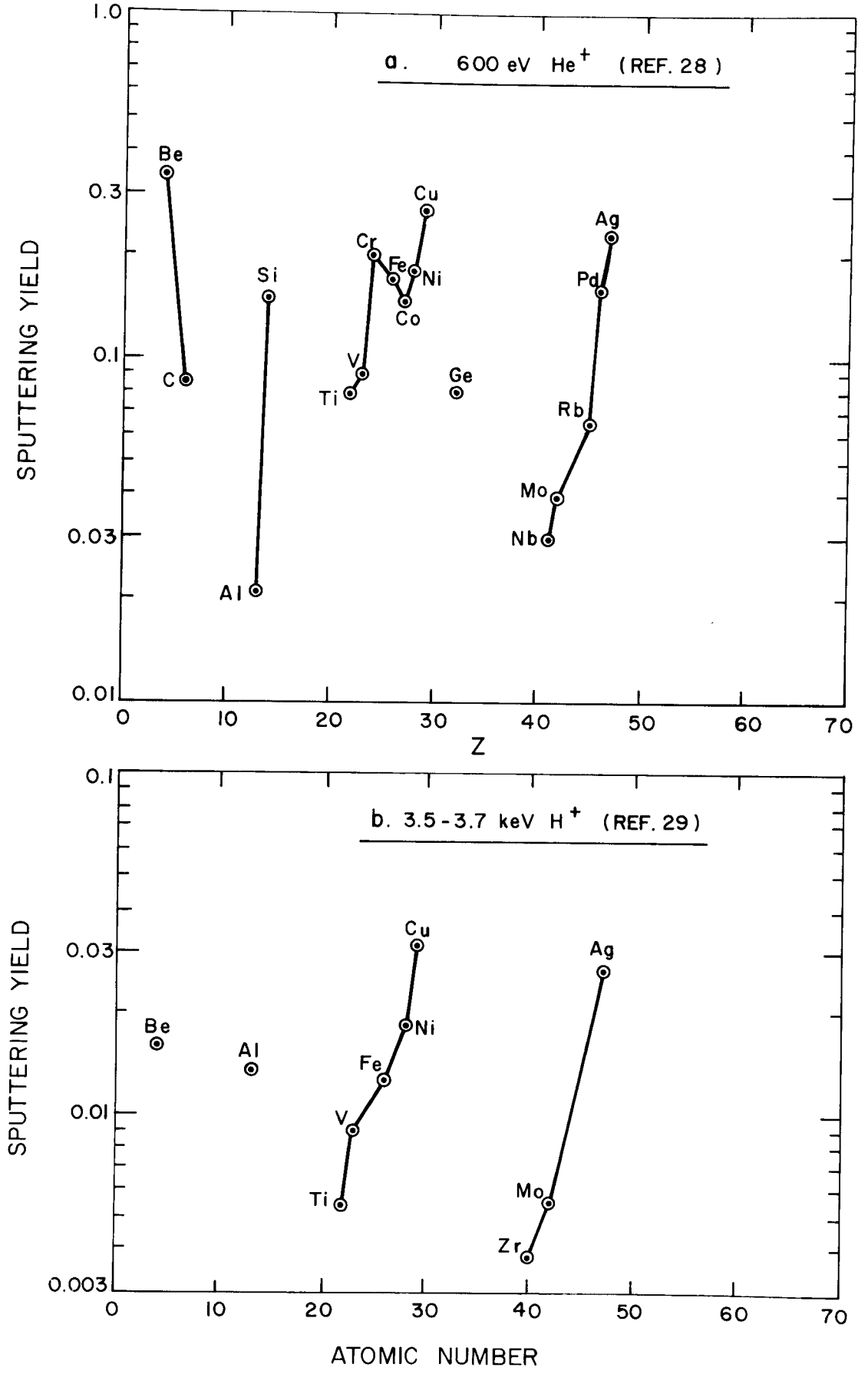
a. 600 eV He+ (REF. 28)
SPUTTERING YIELD
1.0
0.3
0.1
0.03
0.01
Be
C
Si
Al
Cu
Cr
Fe
Ni
Co
V
Ti
Ge
Ag
Pd
Rb
Mo
Nb
0
10
20
30
40
50
60
70
Z
b. 3.5-3.7 keV H+ (REF. 29)
SPUTTERING YIELD
0.1
0.03
0.01
0.003
Be
Al
Cu
Ni
Fe
V
Ti
Ag
Mo
Zr
0
10
20
30
40
50
60
70
ATOMIC NUMBER

FIGURE 1

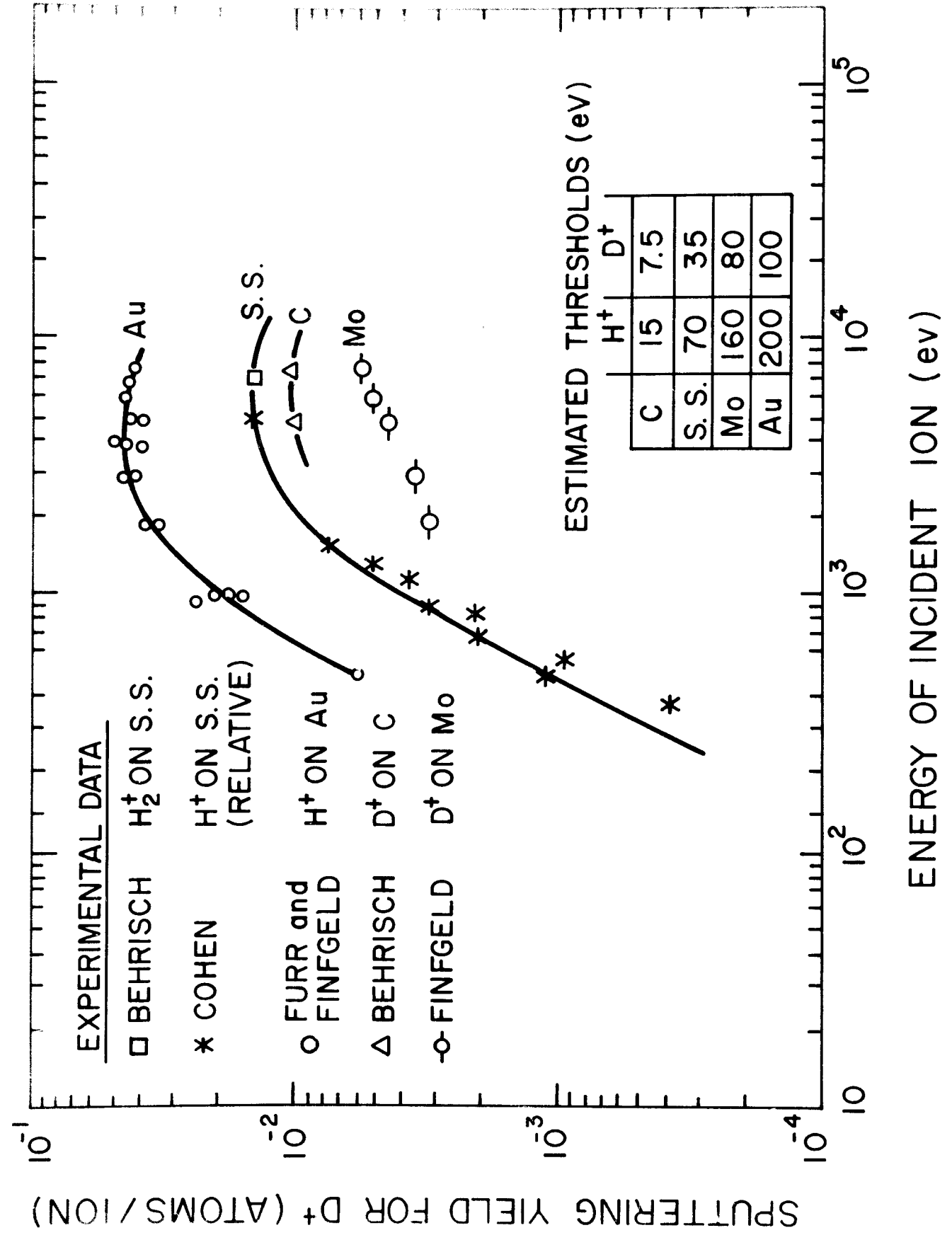
SPUTTERING YIELD FOR D+ (ATOMS/ION)
ENERGY OF INCIDENT ION (ev)
EXPERIMENTAL DATA
□ BEHRISCH H2+ ON S.S.
* COHEN H+ ON S.S. (RELATIVE)
○ FURR and FINFGELD H+ ON Au
△ BEHRISCH D+ ON C
◇ FINFGELD D+ ON Mo
ESTIMATED THRESHOLDS (eV)
H+ D+
C 15 7.5
S.S. 70 35
Mo 160 80
Au 200 100
Au
S.S.
C
Mo

FIGURE 2

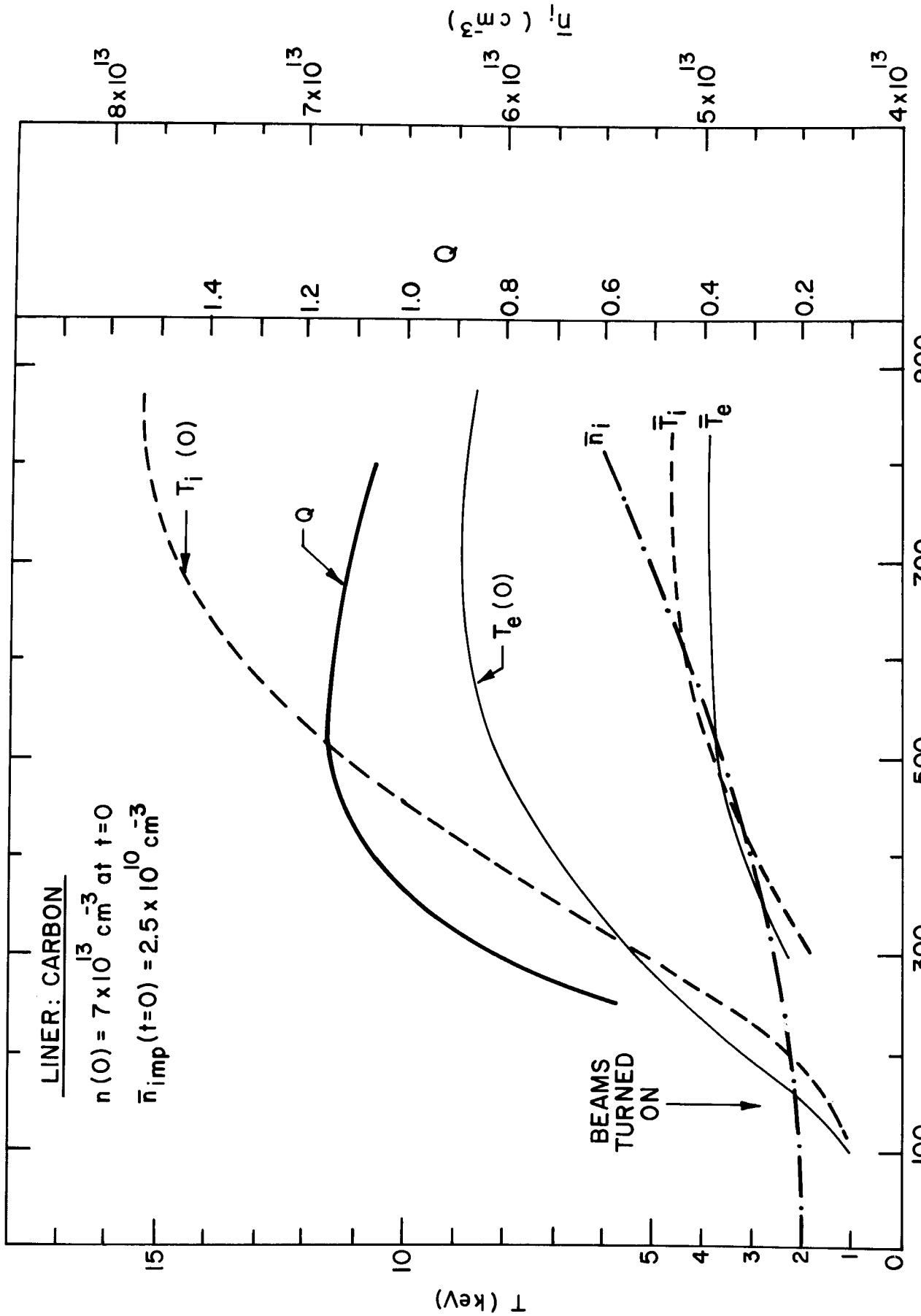
LINER: CARBON
n (0) = 7 x 10^13 cm^-3 at t=0
n̄imp (t=0) = 2.5 x 10^10 cm^-3
Ti (0)
Q
Te (0)
n̄i
T̄i
T̄e
BEAMS TURNED ON
T (keV)
TIME (msec)
Q
n̄i (cm^-3)

FIGURE 3

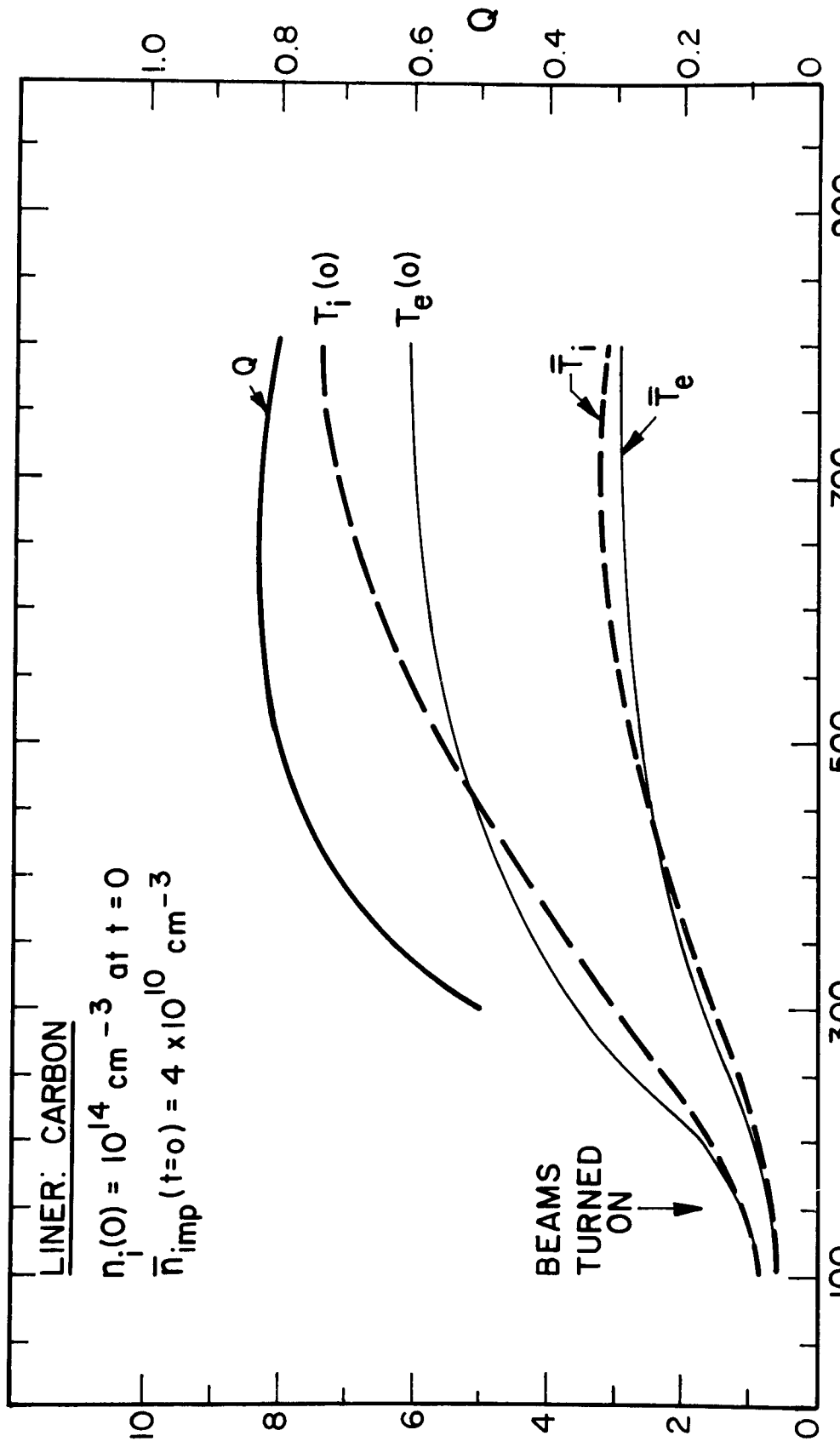
LINER: CARBON
$n_i(0) = 10^{14}$ cm^{-3} at t = 0
$\bar{n}_{imp}(t=0) = 4 \times 10^{10}$ cm^{-3}
Q
$T_i(0)$
$T_e(0)$
$\bar{T}_i$
$\bar{T}_e$
BEAMS TURNED ON
T (keV)
Q
TIME (msec)
0
2
4
6
8
10
0
0.2
0.4
0.6
0.8
1.0
100
300
500
700
900

FIGURE 4

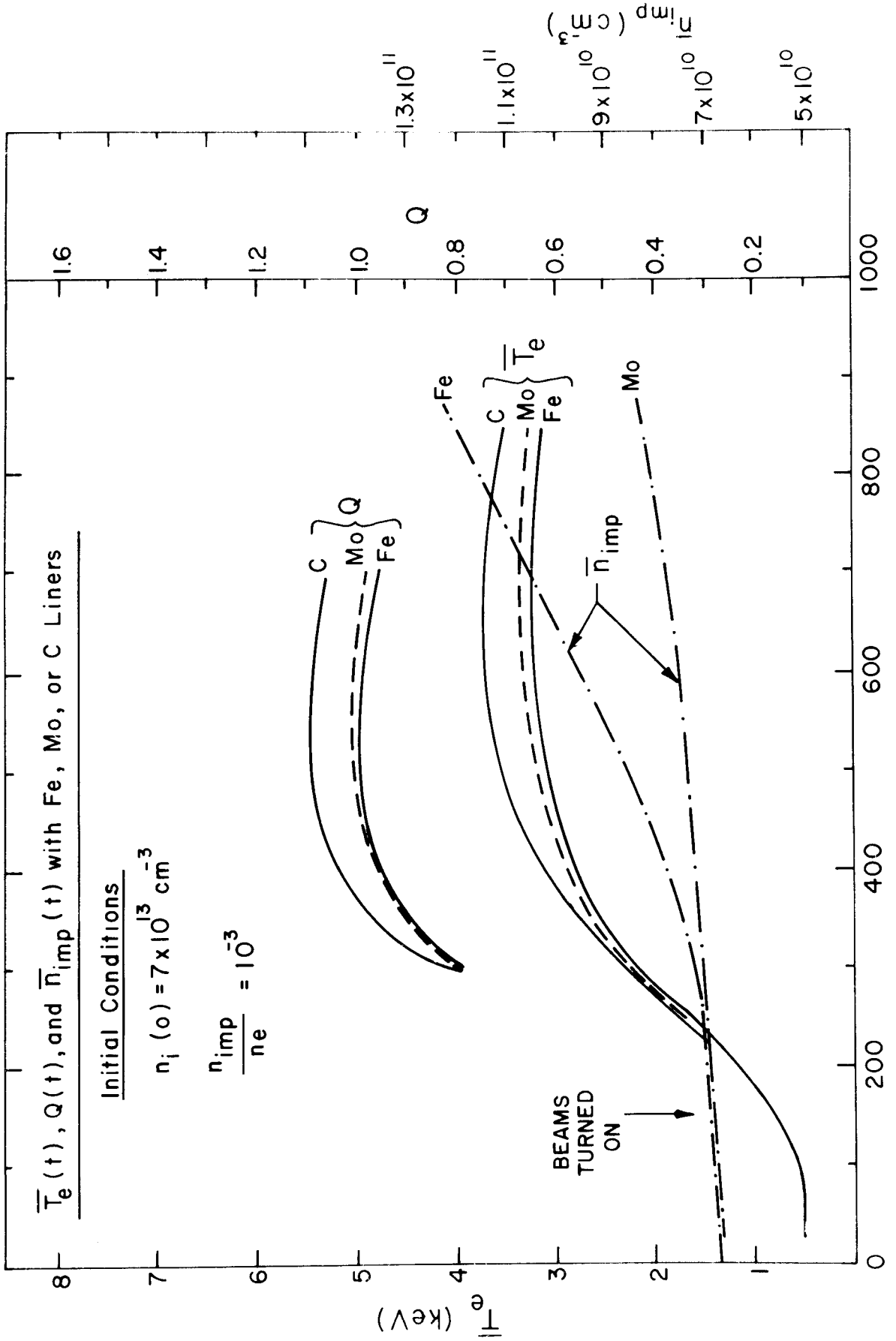
$\overline{T_e}(t)$, Q(t), and $\overline{n}_{imp}(t)$ with Fe, Mo, or C Liners
Initial Conditions
$n_i(o) = 7 \times 10^{13}$ cm^{-3}
$\frac{n_{imp}}{ne} = 10^{-3}$
C
Mo
Fe
Q
$\overline{T_e}$
$\overline{n}_{imp}$
BEAMS TURNED ON
$\overline{T_e}$ (keV)
TIME (msec)
Q
$\overline{n}_{imp}$ (cm^{-3})
0
200
400
600
800
1000
1
2
3
4
5
6
7
8
0.2
0.4
0.6
0.8
1.0
1.2
1.4
1.6
5×10^{10}
7×10^{10}
9×10^{10}
1.1×10^{11}
1.3×10^{11}

FIGURE 5

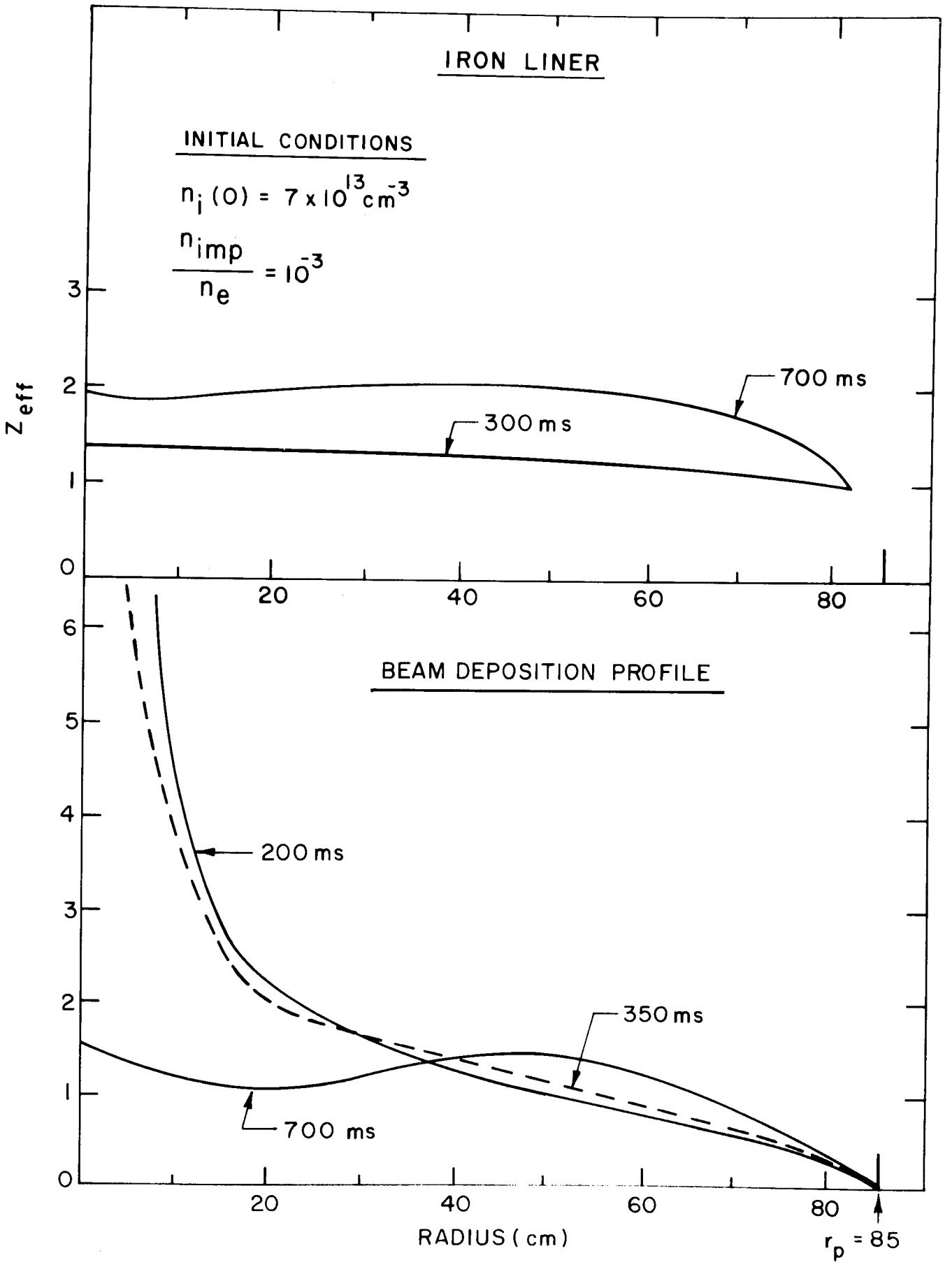
IRON LINER
INITIAL CONDITIONS
$n_i(0) = 7 \times 10^{13}\ cm^{-3}$
$\frac{n_{imp}}{n_e} = 10^{-3}$
Z_{eff}
700 ms
300 ms
BEAM DEPOSITION PROFILE
200 ms
350 ms
700 ms
RADIUS (cm)
$r_p = 85$

FIGURE 6

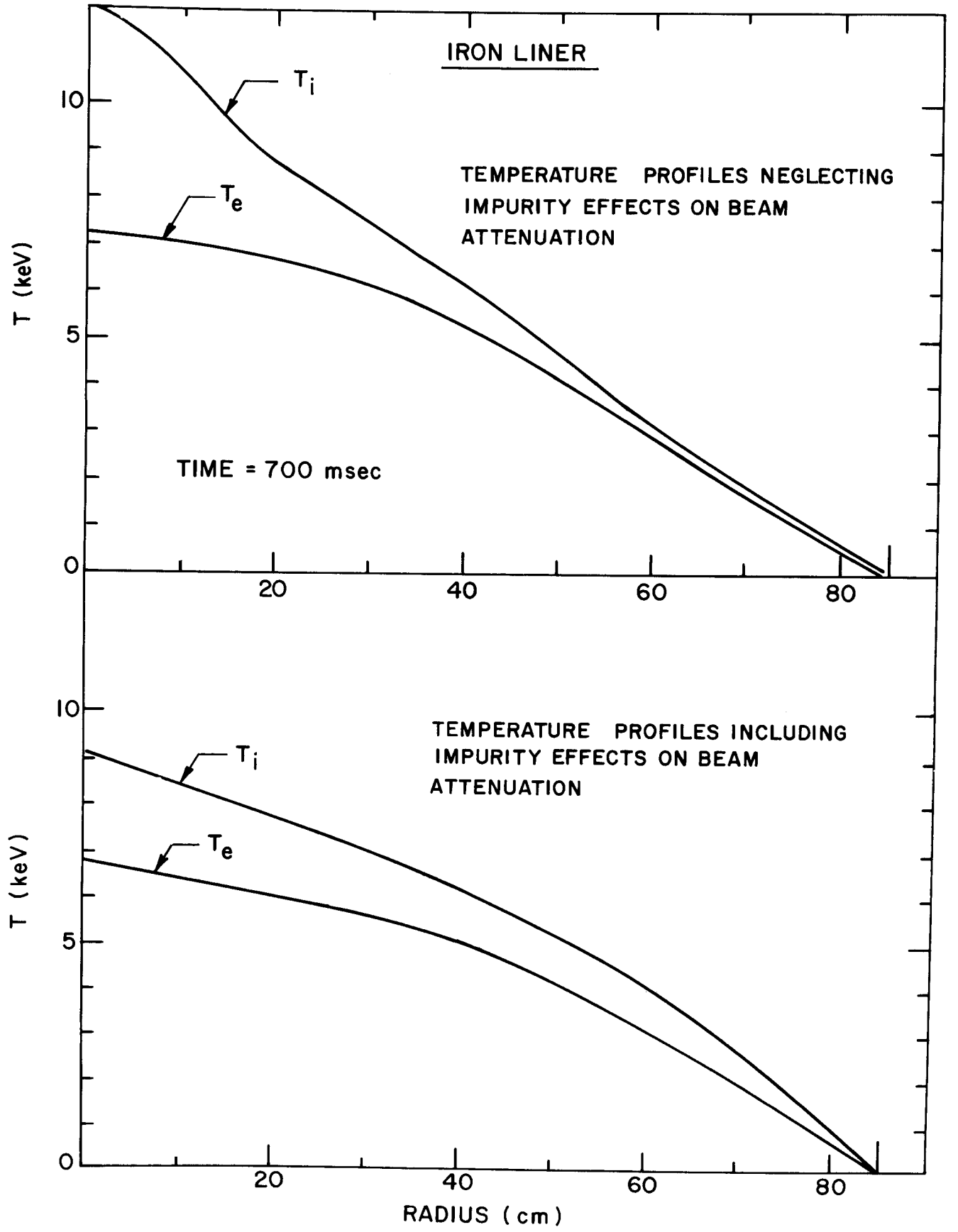
IRON LINER
T_i
T_e
TEMPERATURE PROFILES NEGLECTING IMPURITY EFFECTS ON BEAM ATTENUATION
TIME = 700 msec
T (keV)
10
5
0
20
40
60
80
TEMPERATURE PROFILES INCLUDING IMPURITY EFFECTS ON BEAM ATTENUATION
T_i
T_e
T (keV)
10
5
0
20
40
60
80
RADIUS (cm)

FIGURE 7

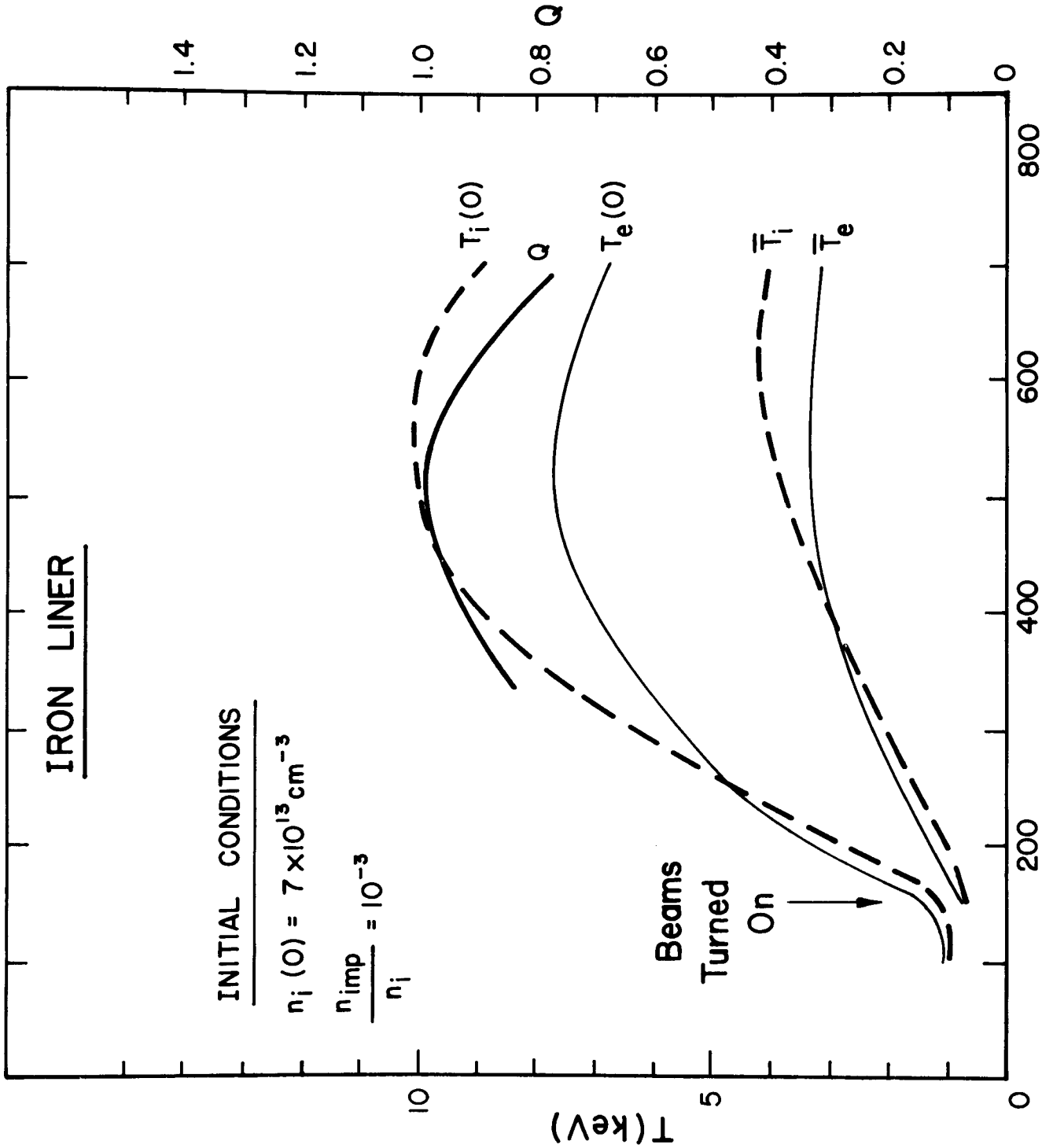
IRON LINER
INITIAL CONDITIONS
$n_i(0) = 7 \times 10^{13} cm^{-3}$
$\frac{n_{imp}}{n_i} = 10^{-3}$
Beams Turned On
$T_i(0)$
Q
$T_e(0)$
$\bar{T}_i$
$\bar{T}_e$
T (keV)
Q
TIME (msec)
0
5
10
0.2
0.4
0.6
0.8
1.0
1.2
1.4
200
400
600
800

FIGURE 8

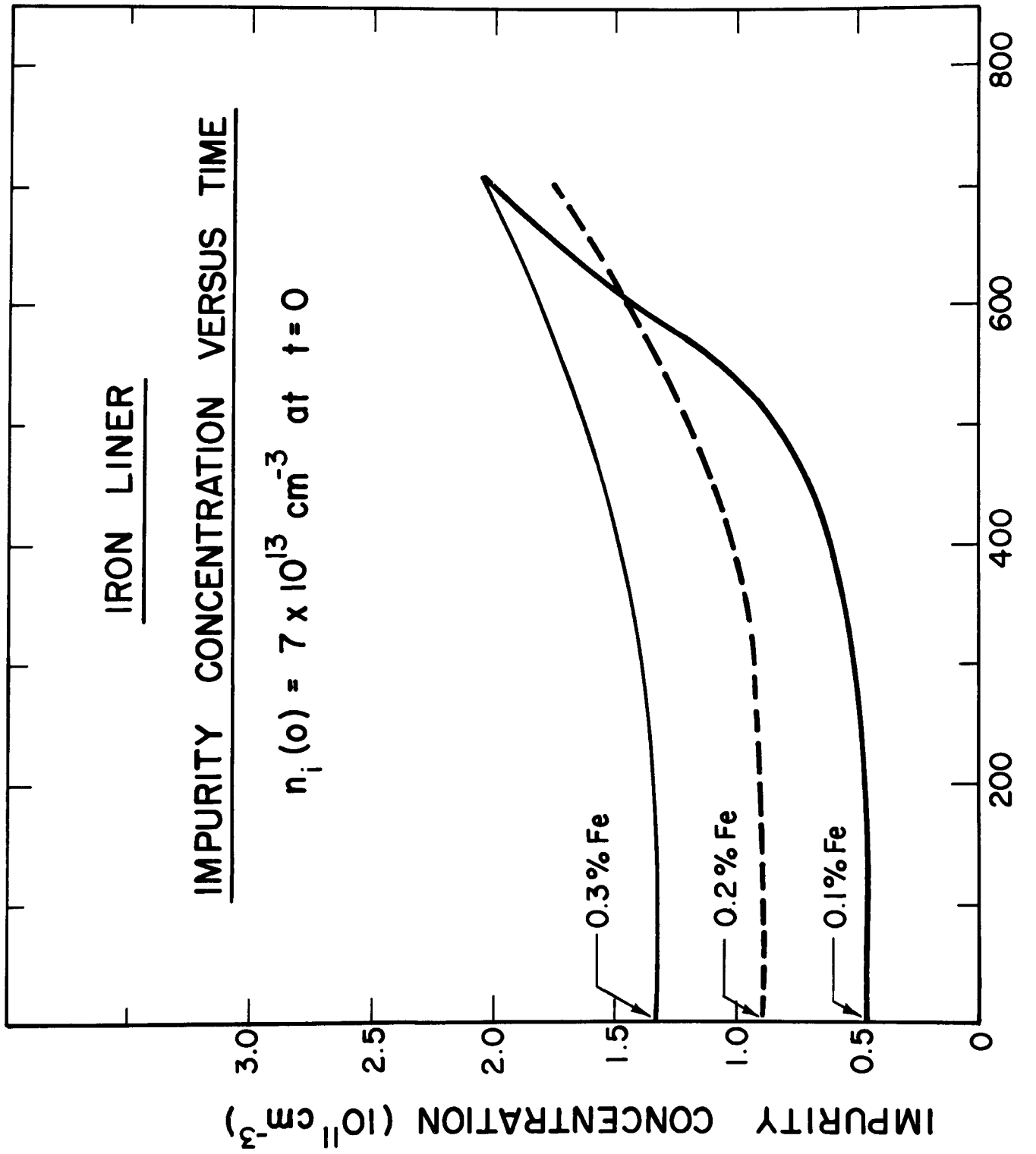
IRON LINER
IMPURITY CONCENTRATION VERSUS TIME
$n_i(o) = 7 \times 10^{13}$ cm^{-3} at t = 0
0.3% Fe
0.2% Fe
0.1% Fe
IMPURITY CONCENTRATION (10^{11} cm^{-3})
TIME (msec)
0
200
400
600
800
0.5
1.0
1.5
2.0
2.5
3.0

FIGURE 9

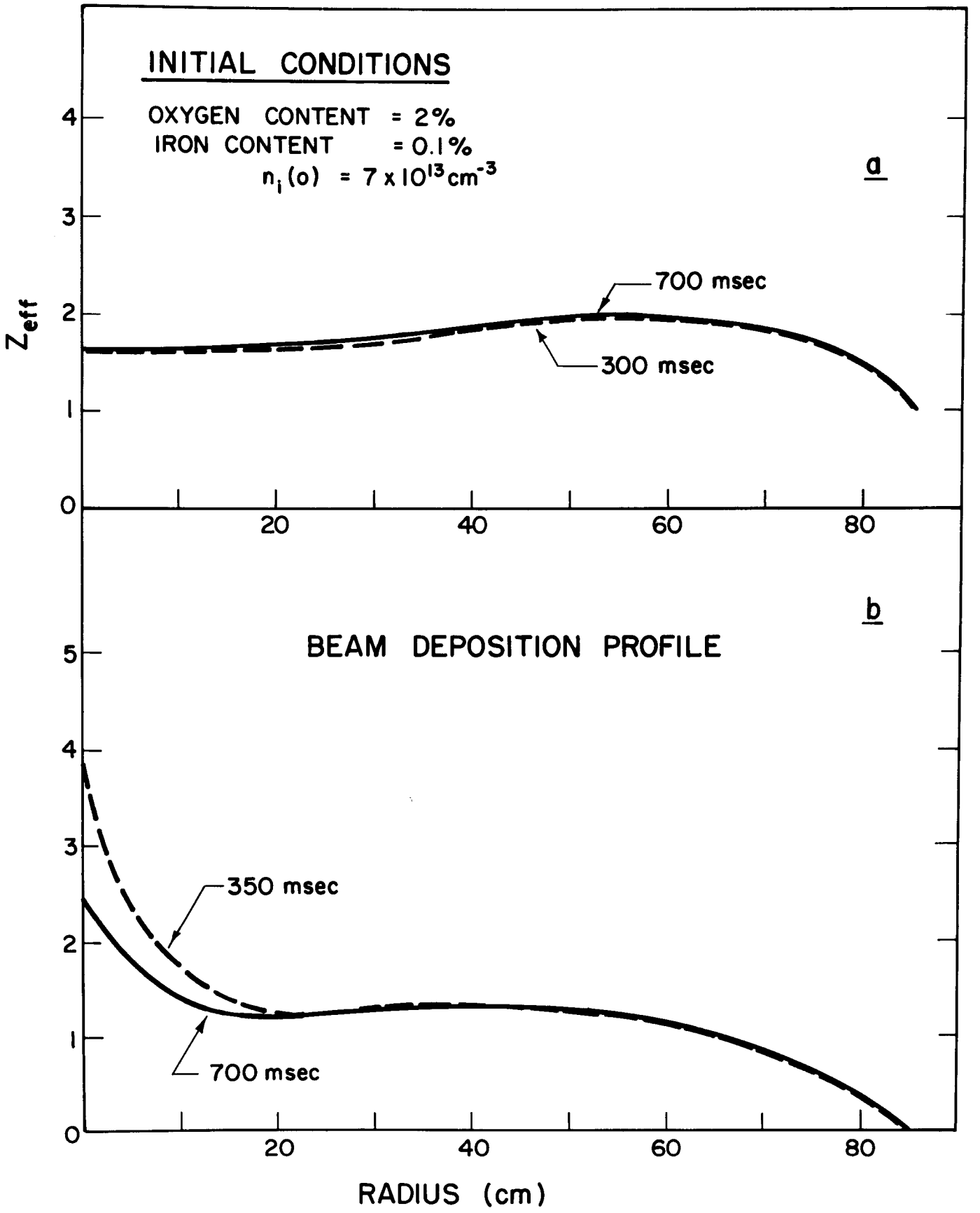
INITIAL CONDITIONS
OXYGEN CONTENT = 2%
IRON CONTENT = 0.1%
$n_i(o) = 7 \times 10^{13} cm^{-3}$
a
700 msec
300 msec
Z_{eff}
0
1
2
3
4
20
40
60
80
b
BEAM DEPOSITION PROFILE
350 msec
700 msec
0
1
2
3
4
5
20
40
60
80
RADIUS (cm)

FIGURE 10

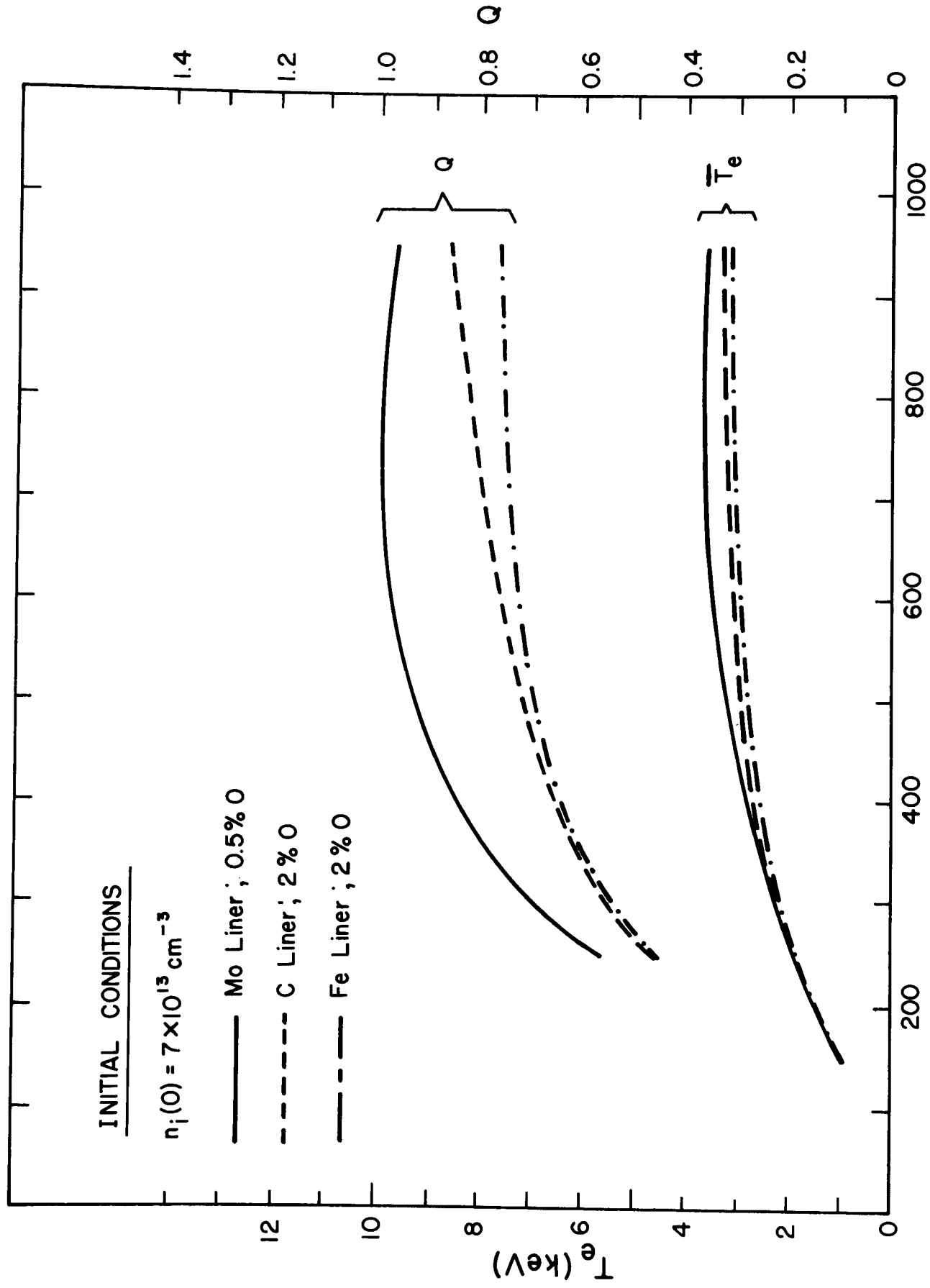
INITIAL CONDITIONS
$n_i(0) = 7 \times 10^{13}\ cm^{-3}$
Mo Liner ; 0.5% O
C Liner ; 2% O
Fe Liner ; 2% O
T_e (keV)
Q
$\bar{T}_e$
TIME (msec)
Q

FIGURE 11

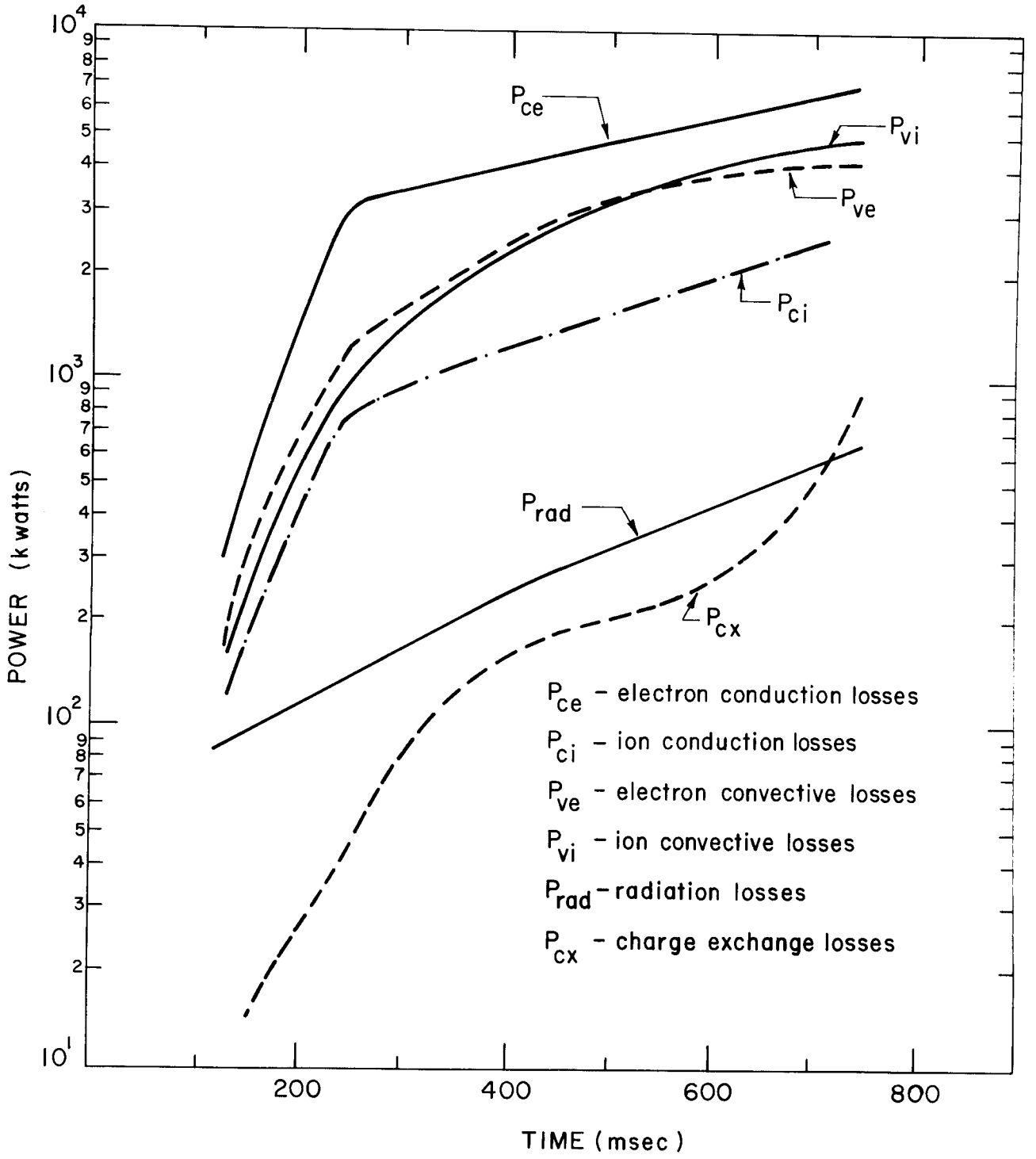
POWER (k watts)
TIME (msec)
P_{ce}
P_{vi}
P_{ve}
P_{ci}
P_{rad}
P_{cx}
P_{ce} - electron conduction losses
P_{ci} - ion conduction losses
P_{ve} - electron convective losses
P_{vi} - ion convective losses
P_{rad} - radiation losses
P_{cx} - charge exchange losses

FIGURE 12

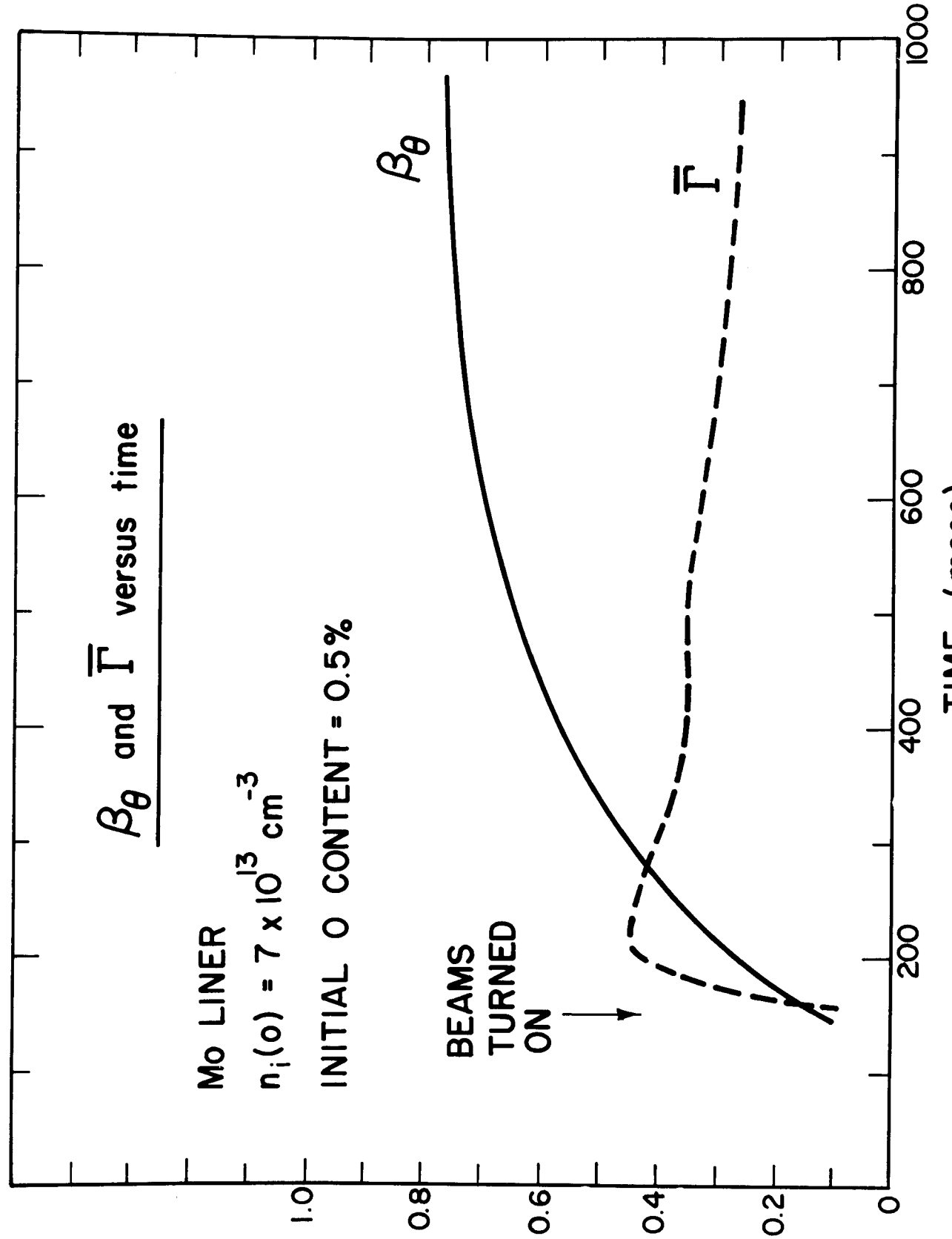
β_θ and $\bar{\Gamma}$ versus time
Mo LINER
$n_i(o) = 7 \times 10^{13}$ cm^{-3}
INITIAL O CONTENT = 0.5%
BEAMS TURNED ON
β_θ
$\bar{\Gamma}$
1.0
0.8
0.6
0.4
0.2
0
200
400
600
800
1000
TIME (msec)

FIGURE 13

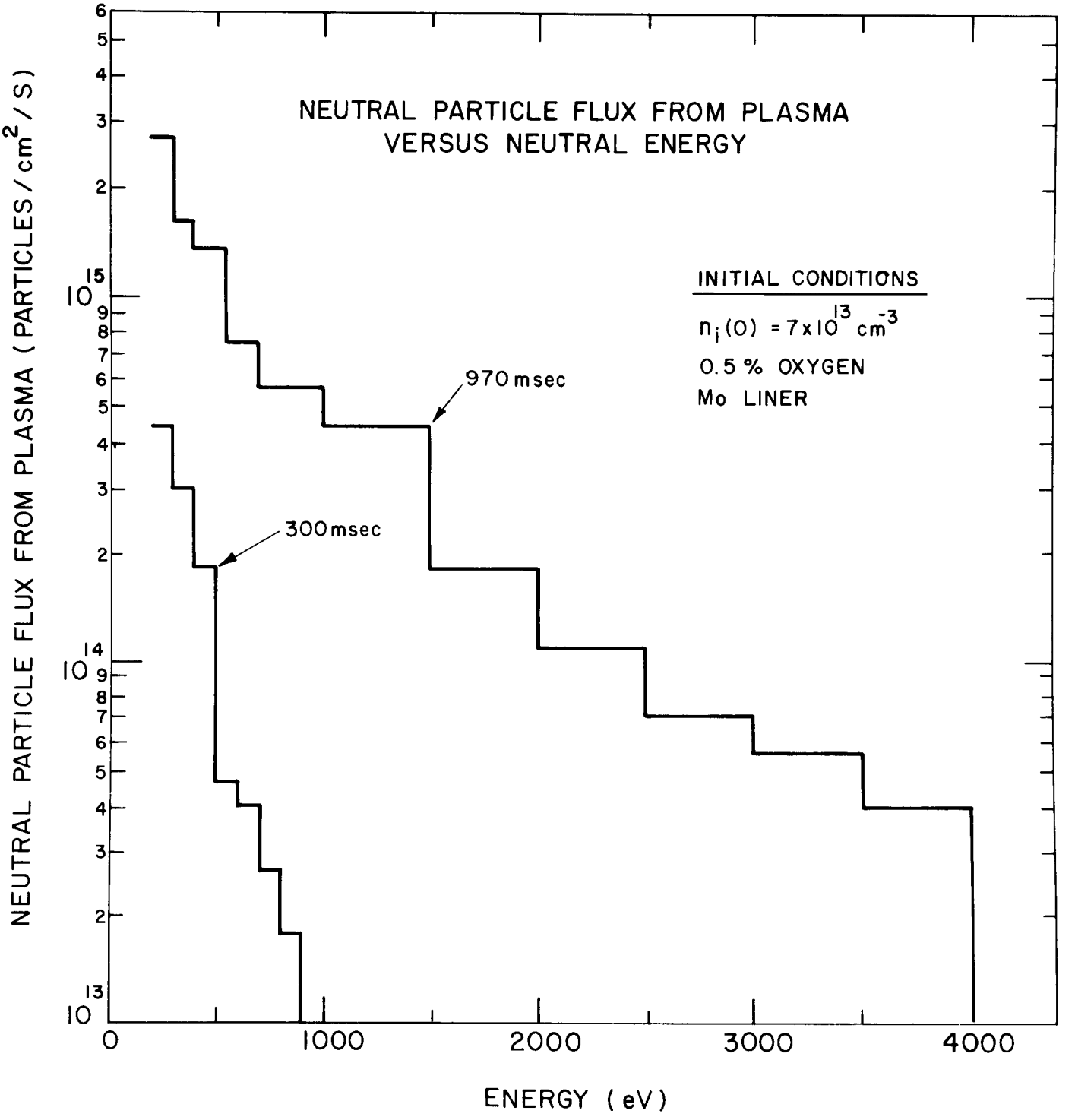
NEUTRAL PARTICLE FLUX FROM PLASMA VERSUS NEUTRAL ENERGY
INITIAL CONDITIONS
$n_i(0) = 7 \times 10^{13}$ cm^{-3}
0.5 % OXYGEN
Mo LINER
970 msec
300 msec
NEUTRAL PARTICLE FLUX FROM PLASMA (PARTICLES / cm^2 / S)
ENERGY (eV)
0
1000
2000
3000
4000

FIGURE 14

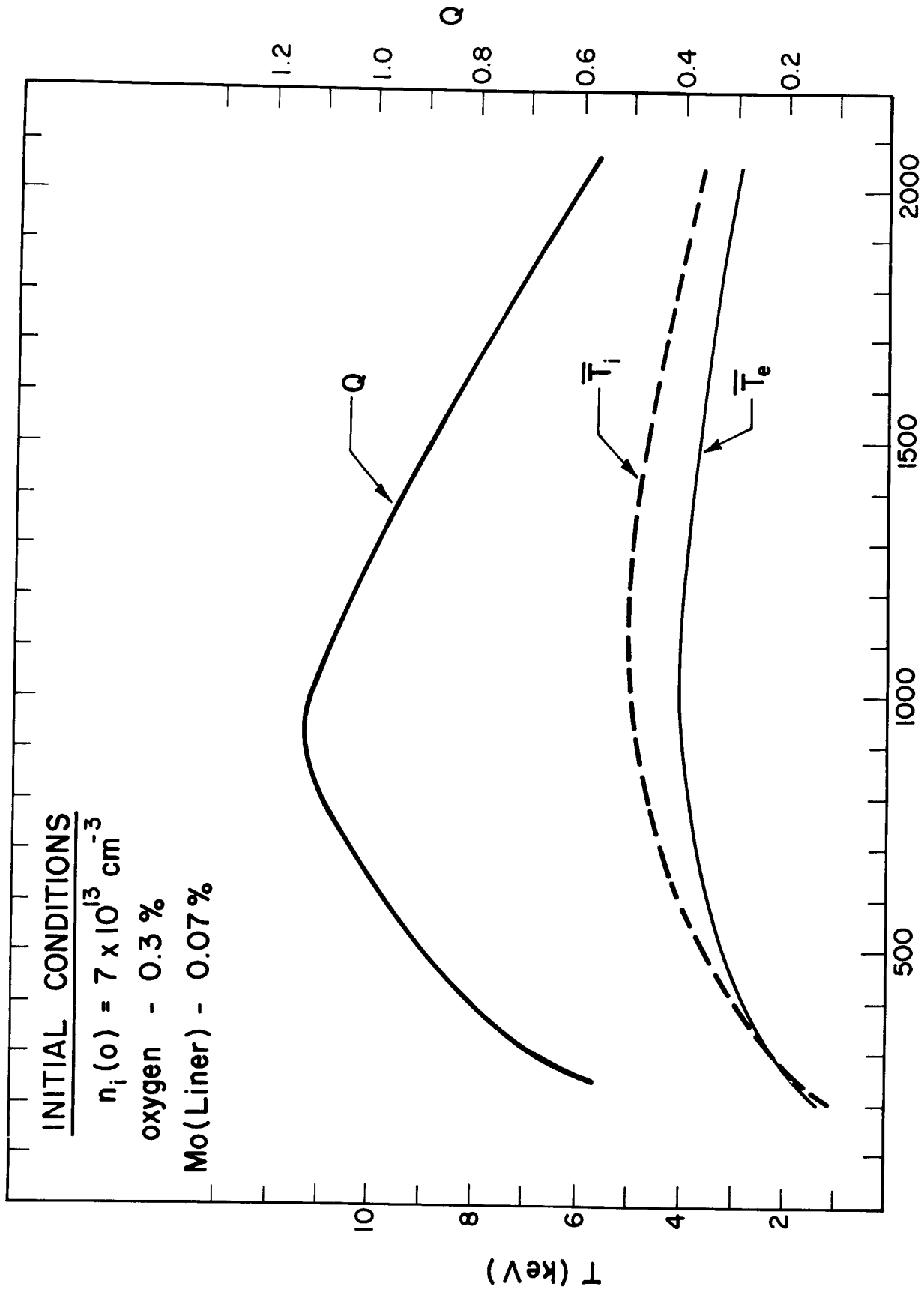
INITIAL CONDITIONS
$n_i(o) = 7 \times 10^{13}$ cm^{-3}
oxygen - 0.3 %
Mo(Liner) - 0.07 %
Q
$\bar{T}_i$
$\bar{T}_e$
T (keV)
TIME (msec)
Q
2
4
6
8
10
500
1000
1500
2000
0.2
0.4
0.6
0.8
1.0
1.2

FIGURE 15